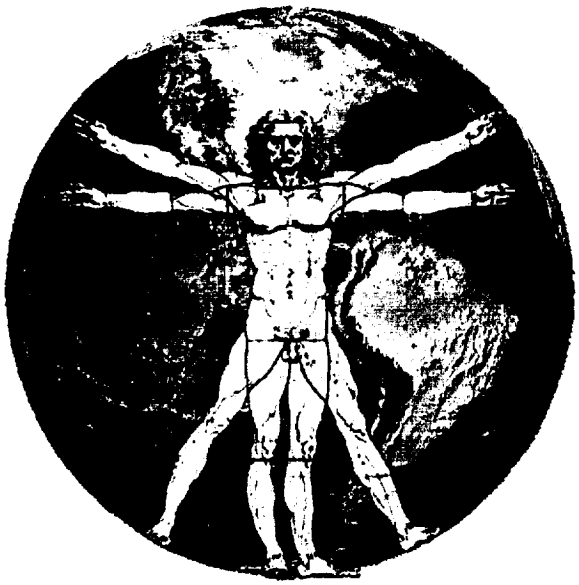

Proxemy Research Technical Report #101-004

Author: Dr. Lori S. Glaze

Title: Quarterly Report: 'Volcanic Plumes on Io and Mars'

Submitted to: Dr. David Senske/COTR
Code SR
NASA Headquarters

December 31, 2001

20528 Farcroft Lane ● Laytonsville, MD 20882 ● (301) 313-0026 ● E-mail: lori@proxemy.com

Proxemy Research is under contract to NASA to perform science research of volcanic plumes on Io and Mars. The following report constitutes delivery of ***Milestone Event #7*** under NASA contract NASW-00013.

TITLE: Io/Mars Quarterly Progress Report #I01-04

AUTHOR: Dr. Lori S. Glaze

1. Introduction

Proxemy Research is under contract to NASA to perform science research of volcanic plumes on Io and Mars. Funding for this project began in May 2000 under contract NASW-00013. The project covered by this contract is comprised of two distinct tasks that were outlined in the original proposal entitled "Volcanic plumes on Io and Mars," dated May 1999. The objective of the first task was to develop a model that constrains stochastic-ballistic effects of variable ejection velocities on areal concentrations of volcanic deposits on Io. The objective of the second task was to apply a buoyant plume rise model to explosive volcanic eruption columns released into an early Mars atmosphere.

2. Quarterly Report

Tremendous progress was made in the last quarter of 2001. Over this three month period, efforts were directed toward three primary activities: (1) submission of a manuscript describing the limits of volcanic plume rise models to conditions on Mars [Attachment A], (2) preparation of a manuscript in collaboration with Ellen Stofan and others describing a statistical analysis of coronae on Venus, and (3) submission of a manuscript in collaboration with Stephen Baloga describing a probabilistic approach to pahoehoe lava flow emplacement [Attachment B]. This last activity has not been funded directly by this contract, but is a collaborative PGG project. Thus it is reported here for completeness.

Volcanic Plumes on Mars

The second task of this contract is intended to focus on the application of plume rise models to explosive volcanic eruptions on Mars. The task considers both current and paleo-atmospheric conditions. Over the last two years, it has become clear that in the past terrestrial plume rise models have been applied to Mars without ensuring the validity of the models themselves. Our studies have shown that the convective rise models that have been used previously break down a few km above the eruption vent. As a result, other studies (e.g., Wilson and Head, 1994; Hort and Weitz, 2001) have overestimated the heights to which volcanic eruption plumes can rise.

In early December a manuscript entitled "Volcanic plume heights on Mars: Limits of validity for convective models" was submitted to JGR/Planets. The manuscript, included here as Attachment A, describes where and why these convective rise models break down. We show that basic model assumptions are violated when (1) vertical velocities exceed the speed of sound, (2) radial expansion rates exceed the speed of sound, (3) radial expansion rates approach or exceed the vertical velocity, and (4) plume radius grossly exceeds the plume height. All of these assumptions are easily violated under current atmospheric conditions on Mars. The reason for the model breakdown is that the current Mars atmosphere is not of sufficient density to satisfy the conservation equations. It is likely that second order effects dominate the plume rise dynamics very rapidly.

Coronae on Venus

In late 2000, Proxemy Research was fortunate to employ Dr. Ellen Stofan. Throughout 2001, we have begun to develop several collaborations. One such collaboration has been to statistically analyze coronae on Venus that Dr. Stofan has previously classified in her corona database. Through this analysis, we are able to distinguish between various subpopulations of coronae. We expect to submit this manuscript within the next three months, and will attach the final version at that time.

Pahoehoe lava flows

I have been collaborating with Stephen Baloga on his PGG grant for many years. One of his primary tasks has been to explore a stochastic model for the emplacement of pahoehoe in the "toe" regime. This last quarter saw the submission of a manuscript to JGR/Solid Earth that we have been working on for quite some time. The manuscript, entitled "Pahoehoe transport as a correlated random walk", is included here as Attachment B. The manuscript describes a correlated random walk model that can predict cross sectional profiles that are consistent with pahoehoe toe emplacement. Although this activity has not been funded directly under this contract, it is included here for completeness.

3. References

Hort, M. and C.M. Weitz, Theoretical modeling of eruption plumes on Mars under current and past climates, *J. Geophys. Res., 106*, 20,547-20,562, 2001.

Wilson, L. and J.W. Head III, Mars: Review and analysis of volcanic eruption theory and relationships to observed landforms, *Rev. Geophys., 32*, 221-263, 1994.

Attachment A

Volcanic plume heights on Mars: Limits of validity for convective models

Lori S. Glaze and Stephen M. Baloga, Proxemy Research, 20528 Farcroft Lane, Laytonsville, MD 20882, 301-313-0026, lori@proxemy.com

Submitted to JGR/Planets, December 5, 2001

Abstract. Previous studies have overestimated volcanic plume heights on Mars. In this work, we demonstrate that volcanic plume rise models, as currently formulated have only limited validity in any environment. These limits are easily violated in the current Mars environment, and may also be violated for terrestrial and early Mars conditions. We indicate some of the shortcomings of the model with emphasis on the limited applicability to current Mars conditions. Specifically, basic model assumptions are violated when (1) vertical velocities exceed the speed of sound, (2) radial expansion rates exceed the speed of sound, (3) radial expansion rates approach or exceed the vertical velocity, (4) plume radius grossly exceeds plume height. All of these criteria are violated for the example given here. Solutions imply that the convective rise model is only valid to a height of ~10 km. The reason for the model breakdown is that the current Mars atmosphere is not of sufficient density to satisfy the conservation equations. It is likely that diffusion and other second order effects dominate the dynamics within the first few kilometers of rise. When the same criteria are applied to eruptions into a higher density early Mars atmosphere, we find that eruption rates higher than 1.4×10^9 kg/s also violate model assumptions. This implies a maximum extent of ~65 km for convective plumes on early Mars. The estimated plume heights for both current and early Mars are significantly lower than those previously predicted in the literature. Therefore, global-scale distribution of ash seems implausible.

Introduction

Models of buoyant volcanic plumes have been applied to the Earth (e.g., Glaze et al. [1997]), Venus [Thornhill, 1993; Robinson et al., 1995; Glaze, 1999], Mars [Mouginis-Mark et al., 1988; Wilson and Head, 1994; Kusanagi and Matsui, 1998; Hort and Weitz, 2001], and Triton [Soderblom et al., 1990; Kirk et al., 1990]. These applications develop various inferences about the role of explosive volcanism in the transport and redistribution of volatiles, the character of eruption conditions, and the nature of surface deposits. These inferences are completely dependent on the validity of the underlying physics contained in the plume models.

The role of explosive volcanism in the transport and redistribution of volatiles on Mars is particularly intriguing. The conjectures of a warm and wet paleoclimate [Pollack et al., 1987], possibly capable of sustaining rainfall [Craddock et al., 1998] and standing water [Parker and Currey, 2001], would favor buoyancy driven plumes. This, coupled with morphologic evidence that older volcanic centers were more explosive [Greeley and Spudis, 1981] may have meant a significant role for explosive volcanism in the injection of green-house gases into the atmosphere. Explosive volcanism under such conditions may have been important for the the redistribution of water on a regional basis as well as a factor in the global water budget.

Long runout pyroclastic flows, and other features on Mars may be the result of this type of paleovolcanism. It has been proposed that layered terrain observed in high resolution MOC (Mars Orbiter Camera) images may be ash deposits from enormous volcanic plumes, that mantle broad regions [Malin and Edgett, 2000]. Furthermore, if explosive volcanism on Mars could produce plumes extending hundreds of kilometers into the atmosphere, these plumes could transport volatiles to the outer atmosphere, facilitating atmospheric release through Jeans escape [Chamberlain, 1978].

All of these important planetary science issues cause concern about the limits of validity for buoyant volcanic plume models and the progeny of inferences drawn from their applications. Many inferences, such as distribution of eruption products, are dependent on the maximum predicted plume height. Plume height estimates given in most terrestrial and planetary applications are based on conservation relationships established by Morton et al. [1956] for buoyant convective rise. The basis of the Morton formulation for convective rise is a system of first-order differential equations prescribing the conservation of mass, volume, and momentum. All aspects of turbulence are reflected in a single constant "entrainment" parameter. These models are intended to approximate solutions of the full Navier-Stokes fluid dynamics system. However, they contain many implicit assumptions and they have only been validated for laboratory, and small industrial plumes on Earth.

While there is broad agreement between theory and observations for volcanic plumes on Earth, it is important to remember that the simple first-order models are necessarily limited. This is due, in part, to the fact that buoyant atmospheric plumes display physical processes that are extremely difficult to model for a wide range of circumstances and parameters. Volcanic plumes are turbulent, have horizontal boundaries that are free to respond to internal dynamics, interact intimately with the local ambient atmosphere, and contain a variety of gas, liquid and particle constituents. Also, from an empirical point of view, field measurements of the quantities needed to improve the theoretical models of turbulent atmospheric plumes are extremely difficult to obtain by comparison with laboratory or natural buoyancy (e.g., industrial plumes) experiments with liquids. The application of these models to other more extreme environments, such as those found in planetary settings on Venus and Mars, exacerbates our need to understand exactly under what conditions the models are valid.

Longstanding opinion in the literature is that explosive volcanic eruption plumes extend five times higher on Mars than analogs on Earth for similar eruption rates, and that column collapse occurs at heights twice those on Earth [Wilson and Head, 1994]. Some estimates [Wilson and Head, 1994; Kusanagi and Matsui, 1998; Hort and Weitz, 2001] claim that explosive eruption plumes can climb to heights in excess of 100 km on Mars. This is more than twice as high as the Mount Pinatubo eruption plume, in an atmosphere that is considerably less dense. There are questions about the validity of convective rise models for volcanic plumes on Earth that have never been addressed. These questions become major concerns when models are applied to the Martian environment.

It is our belief that, not only have basic assumptions of the models been violated in many applications found in the literature, but the buoyant plume models have been

extrapolated well-beyond their limits of validity. There are at least 7 areas of concern that limit the validity of plume rise models formulated in this way. These areas of concern are as follows:

1) *Speed of sound violations:* The models are totally inapplicable, despite what has appeared in the literature, when the speed of sound is exceeded (in the vertical or radial directions), or the atmosphere is too thin to permit definition of the speed of sound [Stothers, 1989].

2) *Radial expansion:* The intent of these models is to describe a plume that is moving primarily upward, not outward. As a result, the rate of radial expansion should be small compared to the vertical velocity and the overall plume radius should be small compared to the plume height.

3) *Ambient air availability:* Turbulent convection models implicitly assume that there is enough ambient air for the plume to behave as a continuum. The models also assume that the corresponding dynamic impact of the plume on the atmosphere is negligible.

4) *Instant mixing:* Most volcanic applications of the Morton approach have considered only the bulk properties of the plume. This carries with it the implicit assumption that all changes in pressure, temperature and density within a control volume are felt instantly and simultaneously throughout each horizontal control volume.

5) *Confluent particle and gas flow:* Particles provide the majority of the heat that drives buoyancy. When we assume that particles and gas flow confluently at all times, it is implied that there must be enough gas pressure to suspend the particles and only enough turbulence to do this without ejecting them. In addition, the heat contained in the particles must be made available to the gas. The time required for conductive heating of the gas must be negligible.

6) *Pressure balance:* One of the most basic simplifying assumptions is that the pressure within the plume is the same as without. Exceeding the speed of sound is an obvious violation of the pressure balance assumption, but there are other indicators that the pressure balance assumption is violated even in lower velocity cases, including rotating columns observed in firestorms and industrial plumes.

7) *Diffusion and other second order effects:* Many second-order effects accounted for in the complete Navier-Stokes treatment (such as diffusion of mass, turbulent eddies, momentum and heat) are ignored in the Morton system. In this reduction, all the second-order effects have been compressed into the entrainment constant, α. It is not clear when the ignored second order effects become important, or if the entrainment parameter is indeed constant in different turbulent environments (e.g., Mars).

Thus, the question we hope to answer with this paper is, "What are the limits of validity for the Morton-type convective rise formulation for conditions on Mars?". We begin with a brief review of the approach that has been the most common method for describing volcanic plumes, including the basic assumptions in the original Morton simplification. We then analyze to what extent these assumptions are valid by addressing the concerns listed above. We focus on current atmospheric conditions found on Mars, as well as the Earth and early Mars. Finally, we attempt to answer the questions: how high could a volcanic plume realistically

rise in the current Mars atmosphere, and how high would the same plume go in a 'paleo' atmosphere?

Convective Rise Models

For completeness, we provide here some background and basic information concerning the convective rise models that are referred to throughout this paper. Over the past two decades, several models describing the convective rise of terrestrial volcanic plumes using a system of first-order conservation equations have appeared in the literature [Wilson et al., 1978; Sparks and Wilson, 1982; Sparks, 1986; Woods, 1988, 1993; Glaze and Baloga, 1996; Glaze et al., 1997]. These models are based on the original work of Morton et al. [1956]. Morton et al. attempted to approximate the more complex Navier Stokes approach to modeling small-scale buoyant flows. It is interesting to note, however, that as yet no one has ever shown a direct link between the time-honored Navier-Stokes and the Morton system. Morton et al. approximated the turbulent entrainment of ambient fluid into a convectively rising plume by using an empirical parameter, referred to here as α. This was originally a very innovative approach that side-stepped the complex modeling of both a turbulent plume and the motion of the ambient atmosphere with a free-boundary between them.

The basic set of conservation equations to be examined in this study are taken from Glaze et al. [1997], hereafter referred to as the model. Other models may contain slight differences, but the basic assumptions of Morton et al. [1956] dominate all results. The basis of this approach is the expression for the conservation of mass, given by

$$\frac{d}{dz}\left[\rho_B u r^2\right] = 2\alpha\rho_{aB} u r \qquad (1)$$

Please see the Notation table for definitions of all variables. The entrainment constant, α, appears explicitly in (1), indicating that the mass of ambient fluid entrained is directly proportional to the upward rise velocity of the plume itself.

The momentum conservation equation corresponding to (1) that prescribes the buoyancy relationship with the ambient fluid can be written as

$$\frac{d}{dz}\left[\rho_B u^2 r^2\right] = g\left(\rho_{aB} - \rho_B\right) r^2 \qquad (2)$$

The thermal energy conservation is

$$\rho_B u r^2 C_B \theta\right] = 2\alpha\rho_{aB} u r C_{aB} T - \rho_{aB} u r^2 g\left(\phi_d \quad (3)$$

where the first and second terms on the right hand side describe how the bulk plume temperature changes due to the entrainment of ambient fluid at a different temperature and adiabatic expansion, respectively.

This simplified approach to modeling buoyantly convecting plumes was stimulated by a desire to understand the dynamics of small industrial plumes. To this end, detailed validation studies were conducted (e.g., Briggs [1969]) to ensure that the models could adequately describe the behavior of convecting plumes in the lower troposphere. Similar models have also been applied to the dynamics of firestorms that are sources of enormous heat [Carrier and Fendell, 1983]. Wilson et al. [1978] and Settle [1978] compared model results to observations of volcanic plume rise and concluded that the Morton-type model of

convective rise was broadly applicable to plinian style volcanism on Earth. Sparks et al. [1997] also present data that support the use of convective plume models, such as that shown above, to describe volcanic eruption columns on Earth. These volcanic comparisons focused on smaller, tropospheric plumes. Thus there are still unresolved issues regarding the broad applicability of the Morton style models to volcanic plumes that penetrate the stratosphere. Furthermore, these comparative analyses are not strictly validation studies, as the true eruptive parameters are always unknown.

There are many fundamental assumptions inherent to all the first order models for convective rise [Stothers, 1989]. The most basic of these include the assumptions that the (1) pressure within the plume is the same as ambient for all altitudes (i.e, plume is 'pressure balanced'), (2) plume material is transported primarily upward (i.e., the vertical velocity is large relative to the radial expansion), (3) particles are able to transfer heat instantaneously to the plume gas (heat conduction within the particle is not important), (4) density difference between the plume and ambient fluid is "small" (although neither the absolute difference, nor the difference relative to other parameters, necessary for model validity have ever been quantified), (5) particles and gas move together (e.g., no drag), and (6) ambient atmosphere is of sufficient density that the plume can be treated as a continuum. An implicit corollary to point (1) is that the vertical velocity of the bulk plume must be less than the local speed of sound.

In applying such models to volcanic eruption plumes on Mars, point (6) becomes of critical importance. The very core of the model described above is that the eruption column must convect, not merely rise buoyantly. Buoyancy is simply the result of density differences in fluids. For example, a balloon can rise buoyantly, but it cannot convect. The process of convection requires the entrainment of ambient fluid and, thus, sufficient ambient fluid must be available for convection to occur at all. The existence of sufficient ambient fluid is a subtle requirement. But, without ambient fluid, there is nothing to "entrain".

Comparison of Atmospheric Conditions

We now compare several attributes of the current Mars atmosphere with the Earth and plausible paleo-atmospheric conditions on Mars. We then present several examples illustrating how and when the basic assumptions above break down.

The convective rise models described above are critically dependent on the basic assumption that there is sufficient atmosphere available for entrainment. We know that at some limit in the absence of sufficient atmosphere, the dynamics of the ejected material must be controlled by ballistic behavior, such as that observed on Io [Glaze and Baloga, 2000]. Where and if the transition occurs is very difficult to ascertain, but the point at which the definition of the speed of sound breaks down is certainly an upper limit for a continuum model. Before we can begin looking at the model, however, we must first characterize the atmosphere in which we are trying to convect. In this section we define the basic atmospheric parameters that are important to the assumptions of the convective models and provide comparisons with our own atmosphere on Earth.

Current atmospheric conditions on Mars are significantly different than on Earth. The gravitational force holding the atmosphere is less, the composition is different (primarily CO_2 on Mars vs N_2 and O_2 on Earth), the surface pressure is two orders of magnitude less, and the atmosphere is considerably cooler. While the pressure of the paleo-Mars atmosphere may have been closer to current conditions on Earth, the composition, temperature and gravity still strongly influence convective plume rise.

For comparative purposes, we use the US Standard Atmosphere for Earth (e.g., Handbook of Chemistry and Physics [1955]). For Mars, we use parameters derived by Seif and Kirk [1977]. More recent estimates of atmospheric conditions on Mars derived from the Mars Pathfinder descent [Magalhaes et al., 1999] are similar to the Viking-derived data. For paleo-conditions on Mars, we allow the surface pressure to be the same as Earth, keeping everything else the same as the current Mars atmosphere.

The temperature profiles used in this comparison and in the modeling examples below are shown in Figure 1. The temperature profile for Mars has been simplified for modeling purposes. Pressure profiles, shown in Figure 2, are derived from the expression $P(z) = P(0) \exp(-z/H)$, where $P(0)$ is the surface pressure, and H is the atmospheric scale height. Table 2 summarizes these and other constants assumed for each of the model atmospheres.

The density profile for each atmosphere is strongly controlled by the pressure. To find the density at each step, we have used the ideal gas relationship $\rho_{aB}(z) = P(z)/R_{aB}T(z)$. To get a better feel for the density of each atmosphere, we have calculated the mean free path as a function of altitude. The mean free path is the average distance that a molecule travels before colliding with another molecule. Most introductory physics texts (e.g., Sears and Zemansky [1967]) discuss the mean free path to some extent. The mean free path, L(z), can be estimated using the expression

$$L(z) = \frac{\sin(\pi/4)}{\sigma\, n(z)} \qquad \textbf{(4)}$$

where n(z) is the molecular density:

$$n(z) = \frac{P(z)N}{R_{aB}\, mw\, T(z)} \qquad \textbf{(5)}$$

and N is Avogadro's Number ($N = 6.0225 \times 10^{23}$). For consistency with the Handbook of Chemistry and Physics, we have used $\sigma = 4.165 \times 10^{-15}$ cm^2 in (4).

Figure 3 is a plot of the mean free path as a function of altitude on both Earth and Mars. For illustrative purposes, we have highlighted a few interesting things as well. First, we have indicated the maximum estimated altitude of the Pinatubo column from the 1991 explosive eruption of ~ 35 - 40 km [Self et al., 1994]. While other eruptions produced larger volumes than Pinatubo, there is no evidence that plumes from these eruptions would have extended much further into the atmosphere. The maximum plume height during the Krakatau eruption of 1883 has been estimated at ~45 km [Self, 1992]. The eruption plume from Toba (73,500 bp), the largest known explosive volcanic event of the late Quaternary, has been estimated at only 27 - 37 km [Rampino and Self, 1992]. The seeming coincidence that all these plumes seem to have similar maximum heights

suggests that there may be some empirical terrestrial limit around 40 km that is not explained by current plume models.

The mean free path at this empirical terrestrial limit is very similar to the mean free path at the surface on Mars. The range of mean free paths where we see convecting plumes on Earth is between 10^{-3} and 10^{-5} cm. Out of interest, we have also highlighted the fact that the average distance between molecular collisions at altitudes where convective plume rise has been predicted on Mars is 1 - 100 meters! Convectively rising plumes must quickly attain an internal density that is similar in magnitude to the ambient atmosphere. This means that at these extreme altitudes, the volcanic plume must also have a mean free path equivalent to the atmosphere at that height. Intuitively, it seems unlikely that particles that must travel even a meter before a collision are capable of entraining anything.

We have also indicated that even the U2 aircraft can only fly as high as about 22 km. Beyond this altitude, there is not enough atmosphere to create aerodynamic lift. Eyewitness accounts of atomic bomb tests indicate that these powerful blasts cannot produce plumes that exceed 9 - 12 km. Furthermore, the firestorm of Hamburg, Germany, in 1943 attained temperatures in excess of 1000 C for a prolonged period, perhaps as much as 6 hrs. Some estimates suggest the temperature may have reached 3000 C, yet the plume only attained a height of 9-12 km kilometers [Carrier and Fendell, 1983].

The most basic assumptions of the convective rise models is that of balanced pressure inside and outside the plume. One of the most obvious ways to violate this assumption is to have vertical rise or radial expansion velocities that exceed the speed of sound. Haliday and Resnick [1977] give the speed of sound as

$$v(z) = \sqrt{\frac{\gamma P(z)}{\rho_{aB}(z)}} \qquad \textbf{(6)}$$

where γ is the ratio of specific heats (Table 2). For N_2 and O_2 which make up 98.9% of Earth's atmosphere, $\gamma = 1.4$. For a primarily CO_2 atmosphere, $\gamma = 1.3$. Figure 4 compares the speed of sound on Earth and Mars. According to the Handbook of Chemistry and Physics, the concept of the speed of sound in Earth's atmosphere loses its applicability at about 90 km where the mean free path of air molecules approaches the wavelengths of sound waves (~ 4 cm). This loss of definition occurs at about 70 km on Mars.

The balanced pressure assumption can also be violated even when plume velocities are less than the speed of sound. Studies of firestorms indicate that the basic pressure balance assumption breaks down with the onset of a rotational motion in the column that is not accounted for by Morton types of formulations. This rotation causes a pressure gradient and may reduce the ability to entrain ambient air (i.e., α) by as much as two orders of magnitude. The validity of Morton formulations has been tested only up to the Long Beach firestorm, which attained a maximum plume height of only several kilometers [Carrier and Fendell, 1983].

Validity Issues

The discussion above regarding ambient atmospheric conditions suggests that there may be some point in Mars' atmosphere where the ambient density is not sufficient for

plumes to rise convectively. Certainly, there is cause for further investigation. The crux of the problem is where to establish the limit of validity for the system of ordinary differential equations in (1) - (3). Here, we attempt to establish where the model breaks down. For the purpose of the following discussions, we will use the basic boundary conditions in Table 3. These are typical boundary conditions that have been used for explosive eruptions on Mars that can be found in the literature (e.g., Hort and Weitz [2001]). For comparison, we have shown the parameters for an eruption on Earth, and into a more dense early Mars atmosphere, with equivalent mass eruption rates. Unless otherwise indicated, the volatile is assumed to be water vapor.

It is critical to this discussion to understand that the model cannot predict the maximum plume height directly because the system of equations (1) - (3) have a singularity at u = 0. As a result of this singularity, both the radius and velocity terms change very rapidly near the top [Glaze and Baloga, 1996]. Previous terrestrial studies have estimated the maximum predicted plume height on Earth by taking the asymptotic solution near this boundary layer. In our previous studies [Glaze and Baloga, 1996; Glaze et al., 1997], this asymptotic solution has been taken as the point at which the upward velocity falls below some set value (usually 10 m/s for large eruptions). On Earth, this cutoff seems to give a reasonable estimate of the limit of validity for the convective rise model. The predicted heights shown in Table 3 correspond to the points at which the velocity falls below 10 m/s as a default case. On Mars, however, this criterion seems insufficient. As can be seen from Table 3, the upward velocity does not drop below 10 m/s until 133 km above the vent. This maximum height is consistent with other predicted plume heights cited in the literature for similar mass eruption rates [Wilson and Head, 1994; Kusanagi and Matsui, 1998; Hort and Weitz, 2001]. The following discussions indicate a variety of other considerations that make applications of the model invalid well below this altitude.

Io Comparison:

We know it is absurd to assume convection on Io where we have visual evidence of ballistic dynamics (e.g., Strom et al. [1981] for early Voyager reports; and Glaze and Baloga [2000] for modeling studies of ballistic dynamics). However, the convective model discussed here cannot make this distinction on its own. If we provide it with boundary conditions, it will attempt to predict convective plume rise, even under absurd conditions.

As an illustration of this, we have run the model for an average Io atmosphere (understanding that the atmosphere on Io changes dramatically between day and night). For modeling purposes, we have assumed an average surface temperature of 110 K that warms slightly with altitude, a surface pressure of 1.7×10^{-8} atm (.0017 Pa), and an atmospheric composition of SO_2. These constraints result in an atmospheric density 10 million times less than Earth. For boundary conditions similar to those on Mars in Table 3 (except gravitational force of 1.8 m s^{-2}), and a magmatic volatile composition that is 50% SO_2 and 50% H_2O, the model blindly predicts that a plume can convect to heights in excess of 150 km on Io.

While we know that explosive eruptions on Io do produce plumes up to 300 km high [McEwen and Soderblom, 1983], the conditions described above would only generate a ~15 km ballistic plume. These

plumes are clearly driven by very different mechanisms than those assumed by the model. For the Mars case then, the primary question is where do the basic assumptions of the convective rise model break down?

Speed of Sound:

One of the most basic assumptions of the convective rise model is that the pressure within the plume is always identically equal to the ambient pressure at that altitude. If the plume is moving slowly enough and if the radius is small enough, this is a plausible assumption. In other words, as long as the time it takes for the effects of the ambient pressure to propagate throughout the entirety of the plume volume is small compared to each time step, this assumption should be reasonable. While it is difficult to identify a specific cutoff where this assumption is violated, it is clearly violated at any point when the vertical rise velocity exceeds the ambient speed of sound.

It has been postulated that initial eruption velocities on Mars may well exceed the speed of sound [Wilson and Head, 1994; Hort and Weitz, 2001]. However, convective rise models should never use such velocities as boundary conditions. As a note, the convective models are not particularly sensitive to the eruption velocity. For example, increasing the initial velocity for Mars in Table 3 to u_o = 500 m/s, the 10 m/s plume cutoff predicts a maximum height of 141 km (a 6% difference). For this study, we only examine results for vent velocities that are below the estimated speed of sound at the surface (~236 m/s).

Figure 5 shows the velocity profile predicted by the convective model using the current Mars boundary conditions defined in Table 3. The general shape of the velocity profile is similar to that predicted for large volcanic eruptions on Earth. For large eruptions, the bulk plume density just above the vent can be significantly greater than the ambient density. Thus, the plume is not buoyant and the column material will slow down as it rises. A convecting plume, however, is simultaneously entraining ambient atmosphere which expands as it is heated by the plume. If the eruption has enough energy, the plume will become buoyant before it loses all of its initial momentum.

The unusual feature of the modeled velocity profile for Mars is that the convectively driven velocity far exceeds the initial eruption velocity. In addition, the upward velocity exceeds even the ambient speed of sound at an altitude of ~34 km. Thus, the convective rise model cannot be valid above this point for two reasons. First, the model in no way accounts for the atmospheric shocks caused by such velocities. Second, continuing past this point certainly violates the basic pressure balance assumption upon which the convective rise model is based.

Radial Expansion:

Ignoring the vertical velocity arguments made above, we need to recall that all the variables in the system of equations (1) - (3) are solved simultaneously. This means that if one wants to accept the predicted plume height given in Table 3, one must be willing to accept ALL the solutions for all the variables given in (1), (2) and (3). In particular, there are several anomalous features of the predicted plume radius that must be accounted for in some way.

The first, and possibly most alarming anomaly, is the predicted radius itself. Figure

6 shows the radial solution that corresponds identically to the velocity solution in Figure 5. If one accepts the final plume height at the point where u < 10 m/s, then one must also accept a plume radius at that point that is in excess of 44,000 km! The circumference of Mars at an altitude of 133 km is ~ 22,000 km, so this would imply that the entire plume top could wrap around Mars four times.

The dramatic increase in the radius implies entrainment of an enormous volume of ambient atmosphere. Aside from the sheer volume of entrained air, the model completely ignores the simultaneous dynamics that would be required for an atmosphere to accommodate this scale of ingestion.

We can immediately see from visual inspection, at the scale of Figure 6, that the radial variable is clearly in a boundary layer regime above 110 - 120 km where the convective model cannot be valid. But where does the radial solution go wrong? Figure 7, shows the radius solution in the altitude range up to about 110 km. However, the radius is already changing very rapidly by about 80 km. This implies that the model may break down even before this point.

To understand what is happening with the radius solution, we have estimated the radial expansion velocity (dr/dt) as a function of altitude. To do this, we simply difference the predicted radius on either side of each step in z. We then divide this Δr by the time it takes the control volume to travel the integration step size (5 m was used in all calculations) using the predicted velocity at that step.

Figure 8 shows the radial expansion velocity along with the vertical velocity and speed of sound for comparison. We see immediately, that the radial expansion velocity exceeds the ambient speed of sound even before the vertical velocity, at a height of ~27 km. It can also be seen from Figure 8 that there is a complex relationship between the vertical and radial velocities. One of the implicit assumptions of the convective rise model is that the primary movement of the plume is upward, not outward (i.e., the radial velocity should be small compared to the vertical). However, the radial velocity far exceeds the vertical velocity at altitudes above ~22 km. In addition, there is some question as to the validity of the initial assumption at heights above ~9 km where the two components almost cross.

The driver that is causing the radial solution to break down is not immediately obvious. Figure 9, however, does shed some light on the issue. In this figure, both the bulk plume density and the ambient atmospheric densities are plotted as functions of altitude. It can be seen from Figure 9 that the plume becomes buoyant (less dense than ambient) at about 10 km. Above that point, the density difference is extremely small (10^{-4} kg/m^3 at 10 km to 10^{-5} kg/m^3 at 50 km). From the form of (2) it can be seen that in order to conserve momentum when (ρ_{aB} - ρ_B) is very small, r must become quite large to compensate. The fact that this density difference is so small raises several important questions. The first is what happens when there are small fluctuations or deviations from our assumptions in the atmospheric conditions? Glaze and Baloga [1996] showed that systematic variation of 2%/km in the cooling rate of a convecting plume can reduce the predicted plume height by 1/3. Furthermore, the model assumes that any changes in plume temperature and density are felt throughout the plume volume instantaneously. For plume radii observed on Earth that exceed several

kilometers, this requires some stretch of the imagination. For plumes with predicted radii exceeding 100's of km on Mars, it seems ridiculous.

Discussion

Based on the discussions above, we believe that volcanic plumes cannot rise convectively to excessive heights in the current Mars atmosphere. For the example given, convection quickly breaks down within the first 10 km. This conclusion is in stark contrast to other studies that predict convective plumes in excess of 100 km. While volcanic plumes may indeed go higher than 10 km, there must be some other mechanism that dominates the transport dynamics.

One possible reason for the breakdown of the convection model is most likely in the exclusion of 2nd order effects, such as diffusion of momentum, turbulence, or energy. It may be that for conditions on Mars, these effects play a much more significant role. Diffusion and rotation serve as an energy sink and may cause the bulk upward velocity of the plume to decrease at a rate greater than predicted by the simplified approach. With the plumes on Mars we have found a unique case where the density difference between the plume and ambient is extremely small, and yet the plume density can never quite "catch up" to the atmosphere. Another possibility is the inability to maintain the confluence of gas and particle motions. As the particles carry the bulk of the heat content, this may dramatically change the internal dynamics of the plume.

Unfortunately, none of this discussion helps us to estimate how high material erupted explosively on Mars may be transported realistically. We can, however, constrain the minimum plausible limits. The first constraint that we can place on plume rise is a minimum estimate based on a purely ballistic vertical trajectory. The maximum height attained by a ballistic mass is solely dependent on the velocity at the vent and gravity, $H = u_o^2/2g$. For a vent velocity of 230 m/s, we can safely say that a plume would have to be a minimum of 7 km high.

Now, one possibility is to apply the convective model up to about 9 km (where we believe we are not violating any basic assumptions), and then allow the plume to continue upward ballistically. At 9 km, the plume density is still greater than the ambient (i.e., not yet buoyant) but, the plume would continue to rise ballistically as a result of its momentum. The model predicts that the plume has a bulk vertical velocity of ~106 m/s at 9 km. Thus, if no more entrainment/convection occurs, the plume would rise an additional 1.5 km, for a total of 10.5 km.

One interesting alternative to consider is the possibility that there is never enough atmosphere for the plume to convect, but that the plume material could still rise due to momentum and buoyancy. This is equivalent to setting the entrainment constant equal to 0.0 (no entrainment). For the initial conditions given in Table 3 and $\alpha = 0$, a plume would rise to a height of about 8 km.

All of these activities lead to the inference that explosive eruptions on Mars could plausibly inject material to altitudes between 10, or perhaps 20 km, under current conditions. The impact of this conclusion is that these eruptions would not be capable of distributing material over significant distances.

It is also of interest to consider eruptions into the early Mars atmosphere.

Assuming a surface pressure of the same order of magnitude as that currently found on Earth, the density of the early Mars atmosphere would have been more dense than our own. The higher density results from bulk gas constants and atmospheric temperatures that are less than Earth. The higher density atmosphere and lower gravity should both result in conditions conducive to convective rise.

But, just how high would we expect plumes to go, and would any of the concerns discussed above become issues? In Table 3 we show the predicted maximum height for a plume with the same mass eruption rate as the example in the current Mars atmosphere. The convective model predicts that this plume would rise to a height of 31 km, about 50% higher than the same plume on Earth. This result is consistent with intuition that plumes should go somewhat higher in a lower gravity, higher density environment. The initial boundary conditions for this example are also within reason, with a vent radius of 100 m, and eruption velocities below the speed of sound. Close inspection of the velocity and radial solution indicates that the violations noted above do not occur under these conditions. Thus, it seems reasonable to model this event as a convecting plume.

We have also explored the possibility of greater eruption rates to determine if there is a limit to how high plumes could go in an early Mars atmosphere. The convective rise model does, indeed, have a limit of 1.4×10^9 kg/s. Mass eruption rates exceeding this limit produce plumes that violate all the criteria discussed for eruptions into the current atmosphere. This mass eruption rate is only 1 order of magnitude greater than the examples give in Table 3, and is equivalent to a vent size of 300 m (with everything else held the same). The maximum predicted plume height resulting from this mass eruption rate is approximately 65 km. Again, this apparent limit is about 50% higher than the empirical limit observed on Earth.

The limit of 65 km under early Mars conditions, while somewhat higher than terrestrial plumes, is probably not sufficient to distribute volcanic ash globally. While aerosols are known to have stayed aloft for months to years following the Pinatubo [Trepte, 1993] and El Chichon eruptions [Pollack et al., 1983], ash particles are believed to have fallen out over a matter of hours to days. The most important implication of this conclusion is that it seems unlikely that volcanoes could be responsible for broad scale mantling and the layered terrain observed in MOC images. Volcanoes could have, however, been major suppliers of volatiles and aerosols into the atmosphere as well as a mechanism for volatile distribution processes.

Conclusions

Based on our analyses, maximum plume heights on Mars extend only a few tens of kilometers and are comparable to those on Earth. Volcanic plumes that rise to heights in excess of 100 km in Mars' current atmosphere are highly improbable. The low density of the current atmosphere simply cannot support convection. The extreme maximum plume heights predicted by other investigators have resulted from a breakdown of the physics model used to describe the plume dynamics. We have demonstrated the breakdown of model validity in a variety of ways:

1) *Speed of sound violations:* The models are totally inapplicable when the speed of sound is exceeded or the atmosphere is too thin to

permit definition of the speed of sound. For the example of a moderately large eruption discussed, we have shown that both the vertical and radial velocity components violate this assumption at 34 km and 27 km, respectively. Thus the model is most certainly invalid at heights above 27 km where no account is made for atmospheric shocks or the fact that the plume is no longer pressure balanced. The assumption of pressure balance may even be violated long before the velocity components exceed the speed of sound (on Earth as well as Mars).

2) *Radial expansion:* One of the most basic, implicit assumptions of convective rise models is that plumes rise primarily upward, not outward. However, the radial expansion velocity of the example plume is of similar magnitude to the vertical velocity by about 9 km, and actually exceeds the vertical velocity at a height of 22 km. In addition, were we to trust the model results above these heights, the radius of the plume quickly exceeds the plume height by orders of magnitude. At a minimum, this excessive expansion indicates that one should be focusing on the radial dynamics, as opposed to vertical. Moreover, the entrained ambient air must be mixed throughout each horizontal cross section of the plume, within the time it takes to travel each time step. As the plume continues to expand, this horizontal mixing assumption becomes increasingly less plausible.

3) *The availability of ambient air:* The reason for excessive radial expansion is that there is not sufficient ambient air available to the plume for entrainment. The density of the atmosphere is so low, that the plume must expand large distances to find sufficient atmospheric mass to satisfy the conservation equation requirements. However, the model in no way accounts for the affect of the plume on the dynamics of the atmosphere. At a minimum, the atmosphere requires separate modeling.

It may well be that volcanoes can inject materials to extreme heights, but it seems highly improbable that convection could possibly be capable. We have shown that for mass eruption rates equivalent to moderately large eruptions on Earth, an eruption plume on Mars could only convect as high as about 9 km. A combination of convection and ballistic transport results in plume heights of only 10 km. It is possible that material produced in explosive volcanic eruptions could go somewhat higher, but it would have to be through some other, mechanism that has not yet been modeled.

An early Mars atmosphere was much more capable of sustaining convecting plumes. Consistent with results of other researchers, an eruption of similar magnitude to the current Mars example would climb to a height of 31 km, ~50% higher than the equivalent plume on Earth. However, there appears to be a limit to the validity of the models on early Mars as well. This limit of validity occurs at an eruption rate of 1.4×10^9 kg/s (1 order of magnitude larger than the 31 km high plume) and produces plumes with a maximum height of 65 km. Eruption conditions exceeding this mass eruption rate violate model assumptions in the same ways as described above.

The net result of these studies is that explosive volcanic eruption plumes can not rise as high as previously projected in the literature. Consequently, injection heights for ash and volatiles have been overestimated, as well as the fall heights of pyroclastic flows. Layered deposits and mantles are currently being recognized in the high resolution Mars images. Conjectures often arise about volcanic

airfall or pyroclastic flows from distant sources. Our results indicate that these sources should not be much farther than analogous deposits on Earth. Whether the current atmosphere or paleo-atmosphere is considered, injection of only a few tens of kilometers into the atmosphere need be considered. Thus, this localization of volcanic effluents implies a local to regional emphasis for volatile transport processes in contrast to large-scale, global atmospheric circulation.

Our recommendation for improving the buoyant plume rise models is to move toward a more generalized form the Navier-Stokes equations, which are second-order, supplemented by appropriate constraining equations (atmosphere, equations of state, etc). It is most essential to begin addressing the diffusion of mass, turbulent eddies, momentum, and heat in the transitional regime, where differences between atmospheric properties (velocities, eddies, heat) are really second-order effects. For the unique conditions on Mars, it may well be that these second-order effects become important within the first 10 - 20 km of rise.

Acknowledgments.

This work was funded by the NASA Planetary Geology and Geophysics (NASW-00013, NAG5-10530, and NAG5-7251) and Solid Earth (NAS5-01009) Programs.

References

Briggs, G.A., *Plume Rise*, 80 pp., U.S. Atomic Energy Comm., Washington, D.C., 1969.

Carrier, G.E., and Fendell, Firestorms, *Am. Soc. Mech. Eng., 25*, 55-64, 1983.

Chamberlain, J.W., *Theory of Planetary Atmospheres*, 330 pp., Academic Press, New York, 1978.

Craddock, R.A., T.A. Maxwell, and A.D. Howard, The evidence for rainfall on early Mars, *Abstracts of the 29th Lunar and Planetary Science Conference*, abstract number 1429, 1998.

Glaze, L.S., Transport of SO^2 by explosive volcanism on Venus, *J. Geophys. Res., 104*, 18,899-18,906, 1999.

Glaze, L.S. and S.M. Baloga, Sensitivity of buoyant plume heights to ambient atmospheric conditions: Implications for volcanic eruption columns, *J. Geophys. Res., 101*, 1529-1540, 1996.

Glaze, L.S. and S.M. Baloga, Stochastic-ballistic eruption plumes on Io, *J. Geophys. Res., 105*, 17,579-17,588, 2000.

Glaze, L.S., S.M. Baloga, and L. Wilson, Transport of atmospheric water vapor by volcanic eruption columns, *J. Geophys. Res., 102*, 6099-6108,1997.

Greeley, R. and P.D. Spudis, Volcanism on Mars, *Rev. Geophys. and Space Phys., 19*, 13-41, 1981.

Haliday, D. and R. Resnick, *Physics, 3rd Edition*, 1131 pp., John Wiley, New York, 1977.

Handbook of Chemistry and Physics, 37th Edition, 3156 pp., Chemical Rubber Publishing Co., Cleveland, 1955.

Hort, M. and C.M. Weitz, Theoretical modeling of eruption plumes on Mars under current and past climates, *J. Geophys. Res., 106*, 20,547-20,562, 2001.

Kirk, R.L., R.H. Brown, and L.A. Soderblom, Subsurface energy storage and transport for solar-powered geysers on Triton, *Science, 250*, 424-429, 1990.

Kusanagi, T. and T. Matsui, The change of eruption styles of martian volcanoes and estimates of the water content of the martian mantle, *Phys. Earth Plan. Interiors, 117*, 437-447, 1998.

Magalhaes, J.A., J.T. Schofield, and A. Seiff,

Results of the Mars Pathfinder atmospheric structure investigation, *J. Geophys. Res., 104,* 8943-8955, 1999.

Malin, M.C. and KS Edgett, Sedimentary rocks of early Mars, *Science, 290,* 1927-1937, 2000.

McEwen, A.S. and L.A. Soderblom, Two classes of volcanic plume on Io, *Icarus, 55,* 191-217, 1983.

Morton, B.R., G.I. Taylor, and J.S. Turner, Turbulent gravitational convection from maintained and instantaneous sources, *Proc. R. Soc. London, Ser. A, 234,* 1-23, 1956.

Mouginis-Mark, P.J., L. Wilson, and J.R. Zimbelman, Polygenic eruptions on Alba Patera, Mars, *Bull. Volcanol., 50,* 361-379, 1988.

Parker, T.J. and D.R. Currey, Extraterrestrial coastal geomorphology, *Geomorphology, 37,* 303-328, 2001.

Pollack, J.B. O.B. Toon, D.J. Hofmann, J.M. Rosen , and E.F. Danielson, The El Chichon volcanic cloud: An introduction, *Geophys. Res. Letts., 11,* 989-992, 1983.

Pollack, J.B., J.F. Kasting, S.M. Richardson, and K. Poliakoff, The case for a wet, warm climate on early Mars, *Icarus, 71,* 203-224, 1987.

Rampino, M.R. and S. Self, Volcanic winter and accelerated glaciation following the Toba super-eruption, *Nature, 359,* 50-52, 1992.

Robinson, C.A., G.D. Thornhill, and E.A. Parfitt, Large-scale volcanic activity at Maat Mons: Can this explain fluctuations in atmospheric chemistry observed by Pioneer Venus?, *J. Geophys. Res., 100,* 11,755-11,763, 1995.

Sears, F.W. and M.W. Zemansky, *University Physics, 3rd printing,* Addison-Wesley Publishing Co., Reading, MA, 1028 pp, 1967.

Seif, A. and D.B. Kirk, Structure of the atmosphere of Mars in summer at mid-latitudes, *J. Geophys. Res., 82,* 4364-4378, 1977.

Self, S, 1992, Krakatau revisited: The course of events and interpretation of the 1883 eruption. Geo-Journal 28.2:109-121.

Self, S., J.-X. Zhao, R.E. Holasek, R.C. Torres and A.J. King, The atmospheric impact of the 1991 Mount Pinatubo eruption, *Fire and mud; eruptions and lahars of Mount Pinatubo, Philippines,* C.G. Newhall and R.S. Punongbayan, editors, University of Washington Press, Seattle, 1089-1115, 1996.

Settle, M., Volcanic eruption clouds and the thermal power output of explosive eruptions, *J. Volcanol. Geotherm. Res., 3,* 309-324, 1978.

Soderblom, L.A., S.W. Kieffer, T.L.Becker, R.H. Brown, A.F. Cook II, C.J. Hansen, T.V. Johnson, R.L. Kirk, and E.M. Shoemaker, Triton's geyser-like plumes: Discovery and basic characterization, *Science, 250,* 410-415, 1990.

Sparks, R.S.J., The dimensions and dynamics of volcanic eruption columns, *Bull. Volcanol., 48,* 3-15, 1986.

Sparks, R.S.J. and L. Wilson, Explosive volcanic eruptions, V, observations of plume dynamics during the 1979 Soufriere eruption, St. Vincent, *Geophys, J. R. Astron. Soc., 69,* 551-570, 1982.

Sparks, R.S.J., M.I. Bursik, S.N. Carey, J.S. Gilbert, L.S. Glaze, H. Sigurdsson, A.W. Woods, *Volcanic Plumes,* John Wiley & Sons, Chichester, 1997.

Stothers, R.B., Turbulent atmospheric plumes above line sources with an application to volcanic fissure eruptions on the terrestrial planets, *J. Atmos. Sci., 46,* 2662-2670, 1989.

Strom, R.G., N.M. Schneider, R.J. Terrile, A.F. Cook, and C. Hansen, Volcanic eruptions on Io, *J. Geophys. Res., 86,*

8593-8620, 1981.

Thornhill, G.D., Theoretical modeling of eruption plumes on Venus, *J. Geophys. Res., 98,*9107-9111, 1993.

Trepte, C.R., R.E. Veiga, and M.P. McCormick, The poleward dispersal of Mount Pinatubo volcanic aerosol, *J. Geophys. Res., 98,* 18,563-18,573, 1993.

Wilson, L. and J.W. Head III, Mars: Review and analysis of volcanic eruption theory and relationships to observed landforms, *Rev. Geophys., 32,* 221-263, 1994.

Wilson, L., R.S. J. Sparks, T.C. Huang, and N.D. Watkins, The control of volcanic column heights by eruption energetics and dynamics, *J. Geophys. Res., 83,* 1829-1836, 1978.

Woods, A.W., The fluid dynamics and thermodynamics of eruption columns, *Bull. Volcanol., 50,* 169-193, 1988.

Woods, A.W., Moist convection and the injection of volcanic ash into the atmosphere, *J. Geophys. Res., 98,* 17,627-17,636, 1993.

Table 1. Notation

Variable	Definition
C_B	Bulk specific heat for plume (J K^{-1} kg^{-1})
C_{aB}	Bulk atmospheric specific heat (J K^{-1} kg^{-1})
g	Acceleration due to gravity (m s^{-2})
H	Maximum plume height (m)
L(z)	Mean free path (m)
mw	Molecular weight (kg/mol)
N	Avogadro's number (6.0225 x 10^{23})
n(z)	Molecular density (molecules m^{-3})
P(z)	Pressure (Pa)
r	Plume radius (m)
R_{aB}	Bulk atmospheric gas constant (J K^{-1} kg^{-1})
T(z)	Atmospheric temperature (K)
u	Vertical plume velocity (m s^{-1})
v	Speed of sound (m s^{-1})
z	Vertical coordinate (m)
α	Entrainment parameter (= .09)
γ	Ratio of specific heats
θ	Bulk plume temperature (K)
ρ_B	Atmospheric density (kg m^{-3})
ρ_{aB}	Bulk plume density (kg m^{-3})
σ	Mean molecular cross sectional area (m^2)
ϕ_d	Fraction of control volume occupied by entrained gas
ϕ_v	Fraction of control volume occupied by magmatic gas

Table 2. Summary of atmospheric parameters.

Parameter	Earth	Mars - current	Mars-paleo
Surface Pressure, P(0)	1.0 atm	.01 atm	1.0 atm
Scale Height, H	7 km	8 km	8 km
Bulk Gas Constant, R_{aB}	287 J K^{-1} kg^{-1}	191 J K^{-1} kg^{-1}	191 J K^{-1} kg^{-1}
Bulk Molecular Weight, mw	28.2 g/mol	43.49 g/mol	43.49 g/mol
Gravity, g	9.8 m s^{-2}	3.7 m s^{-2}	3.7 m s^{-2}
Specific Heat Ratio, $\gamma = C_p/C_v$	1.4	1.3	1.3

Table 3. Boundary conditions used in examples.

Parameter	Earth	Mars-current	Mars-paleo
Radius at Source (r_o)	200 m	1000 m	100 m
Velocity at Source (u_o)	300 m/s	230 m/s	230 m/s
Temperature at Source(θ_o)	1000 K	1000 K	1000 K
Gas Mass Fraction of Magma(n_o)	5%	1%	5%
Mass Eruption Rate ($\rho_o u_o \pi r_o^2$)	1.6 x 10^8 kg/s	1.6 x 10^8 kg/s	1.6 x 10^8 kg/s
Maximum Predicted Height	21 km	133 km	31 km

Figure Captions

Figure 1. Atmospheric temperatures as a function of altitude assumed in model calculations. Temperatures for Earth are for the US Standard Atmosphere. Temperatures for Mars and Paleo-Mars are a simplification of those reported by Sief and Kirk [1977].

Figure 2. Atmospheric pressures as a function of altitude assumed in model calculations. Pressures for Earth are for the US Standard Atmosphere. Pressures for Mars and Paleo-Mars assumed surface pressures of 1.0×10^3 Pa and 1.0×10^5 Pa, respectively. Both profiles assumed a scale height of 8 km.

Figure 3. Mean free path as a function of altitude for Earth, Mars and Paleo-Mars. Also noted are the maximum altitude of the Pinatubo eruption column, the maximum altitude at which the U2 aircraft can fly, and the maximum observed altitudes for atomic bomb tests and firestorms.

Figure 4. Local speed of sound as a function of altitude for Earth, Mars and Paleo-Mars. Note that current and early Mars have similar profiles for speed of sound resulting from the dependence on temperature (we have assumed the same temperature profile for both cases). Also note that the curves stop at some maximum altitude, above which the speed of sound is not defined.

Figure 5. Bulk vertical velocity as a function of altitude for the Mars boundary conditions given in Table 3. The local speed of sound is also shown for comparison.

Figure 6. Solution for plume radius as a function of altitude for the Mars boundary conditions given in Table 3. Note that the radii shown are in kilometers. The full solution corresponding to the velocity solution in Figure 5 is shown.

Figure 7. Solution for plume radius as a function of altitude for the Mars boundary conditions given in Table 3. This is the same solution as that shown in Figure 6, but focused only on radii between 0 and 120 km.

Figure 8. Comparison of radial expansion and vertical velocities for the Mars boundary conditions given in Table 3. Local speed of sound is also shown. Note that the assumption of small radial velocity relative to vertical is violated before the plume reaches 10 km altitude.

Figure 9. Comparison of ambient atmospheric density and bulk plume density, as functions of altitude, for the Mars boundary conditions given in Table 3.

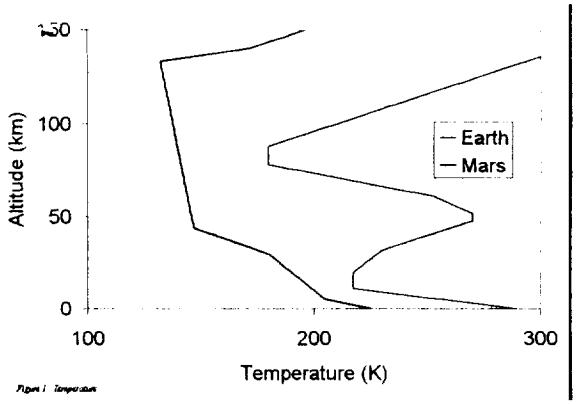
Altitude (km)
150
100
50
0
100
200
300
Temperature (K)
Earth
Mars

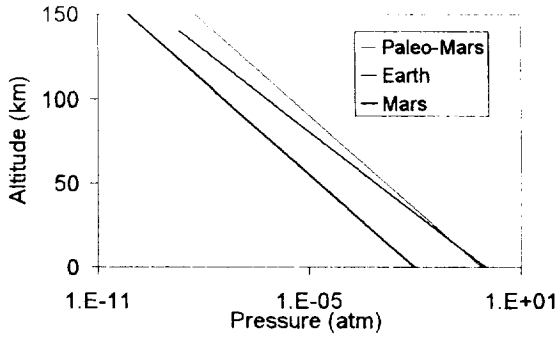
Altitude (km)
150
100
50
0
1.E-11
1.E-05
1.E+01
Pressure (atm)
Paleo-Mars
Earth
Mars

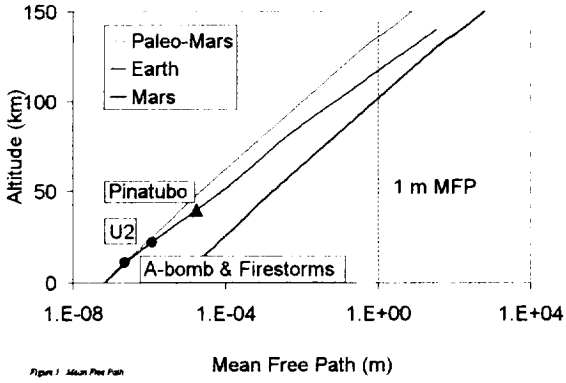
Altitude (km)
150
100
50
0
1.E-08
1.E-04
1.E+00
1.E+04
Mean Free Path (m)
Paleo-Mars
Earth
Mars
Pinatubo
U2
A-bomb & Firestorms
1 m MFP

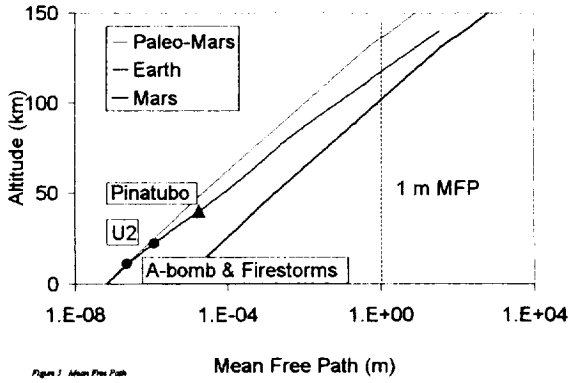
Altitude (km)
150
100
50
0
1.E-08
1.E-04
1.E+00
1.E+04
Mean Free Path (m)
Paleo-Mars
Earth
Mars
Pinatubo
U2
A-bomb & Firestorms
1 m MFP

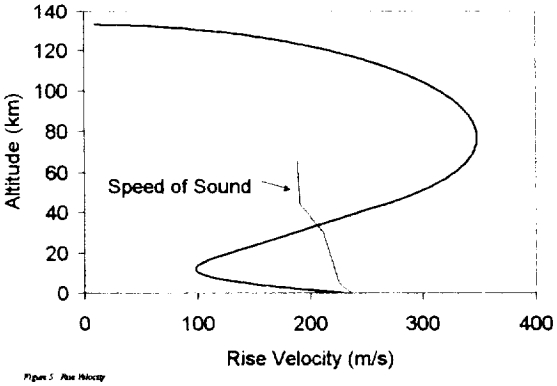
Altitude (km)
140
120
100
80
60
40
20
0
0
100
200
300
400
Rise Velocity (m/s)
Speed of Sound

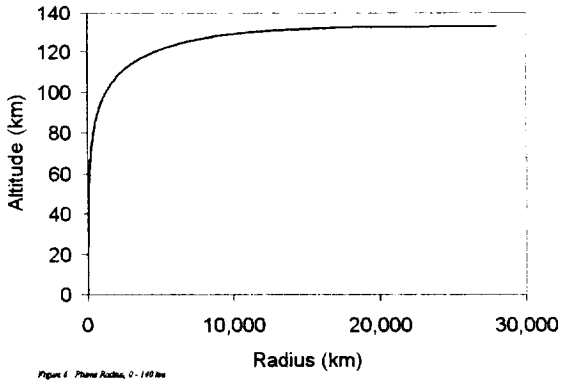
Altitude (km)
140
120
100
80
60
40
20
0
0
10,000
20,000
30,000
Radius (km)

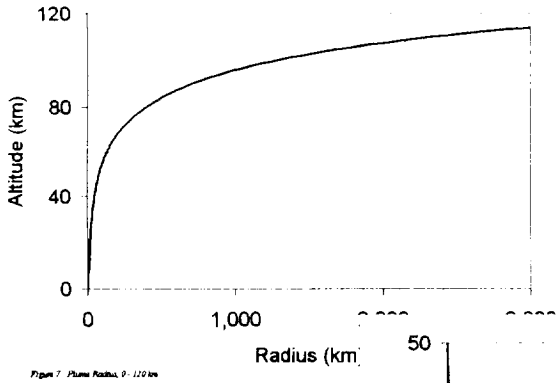
Altitude (km)
120
80
40
0
0
1,000
Radius (km

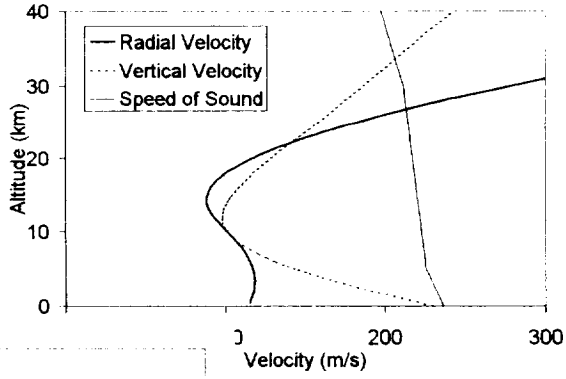
Altitude (km)
40
30
20
10
0
200
300
Velocity (m/s)
Radial Velocity
Vertical Velocity
Speed of Sound

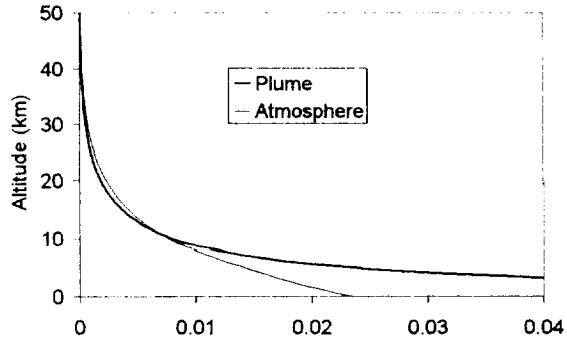
Altitude (km)
50
40
30
20
10
0
0
0.01
0.02
0.03
0.04
Plume
Atmosphere

REPORT DOCUMENTATION PAGE

Form Approved
OMB No. 0704-0188

1. AGENCY USE ONLY *(Leave blank)*	2. REPORT DATE 31 December 2001	3. REPORT TYPE AND DATES COVERED Quarterly Report 10/1/01-12/31/01

4. TITLE AND SUBTITLE Quarterly Progress Report #101-004

5. FUNDING NUMBERS

C NASW-00013

6. AUTHORS Lori S. Glaze

7. PERFORMING ORGANIZATION NAME(S) AND ADDRESS(ES)

Proxemy Research
20528 Farcroft Lane
Laytonsville, MD 20882

8. PERFORMING ORGANIZATION REPORT NUMBER

IO 101-004

9. SPONSORING/MONITORING AGENCY NAME(S) AND ADDRESS(ES)

NASA
Code SR
Washington, D.C. 20546

10. SPONSORING/MONITORING AGENCY REPORT NUMBER

11. SUPPLEMENTARY NOTES

12a. DISTRIBUTION/AVAILABILITY STATEMENT

12b. DISTRIBUTION CODE

13. ABSTRACT *(Maximum 200 words)*

Proxemy Research is under contract to NASA to perform science research of volcanic plumes on Venus and Io. This report is submitted in accordance with contract NASW –00013 and contains a summary of activities conducted over the time period indicated in field 3, above. In addition to a synopsis of science research conducted, any manuscripts submitted for publication in this time period are also attached. Abstracts to scientific conferences may also be included if appropriate.

14. SUBJECT TERMS Venus/IO

15. NUMBER OF PAGES

16. PRICE CODE

17. SECURITY CLASSIFICATION OF REPORT	18. SECURITY CLASSIFICATION OF THIS PAGE	19. SECURITY CLASSIFICATION OF ABSTRACT	20. LIMITATION OF ABSTRACT
Unclassified	Unclassified	Unclassified	SAR

Attachment B

PAHOEHOE TRANSPORT AS A CORRELATED RANDOM WALK

S. M. Baloga and L. S. Glaze, Proxemy Research, 20528 Farcroft Ln, Laytonsville, MD 20882, 301-313-0026, steve@proxemy.com

Submitted to JGR/Solid Earth, December 28, 2001

Abstract. Transport and emplacement of pahoehoe lava is often dominated by random influences, such as budding, small-scale variations in topography, and variations in how the skin cools, stretches, and cracks. We develop a random-walk model to describe the transport of small pahoehoe lobes when random effects are a significant influence on emplacement. We derive a stochastic formalism for random movements on a two-dimensional grid. Our formulation features correlation and bias that determine the degree of randomness in the random walk of each parcel of lava. We compare qualitative and quantitative predictions of the random walk with observations and data for pahoehoe lobes in Hawaii. It is found that a correlated random walk quantitatively describes lobe thickness transects whereas the uncorrelated random walk only reproduces the meandering of small monofilaments of a few toes. Correlation expresses momentum effects and a chain of memory from the front to the source of lava supply. We show that the correlated random walk features a channel-forming regime that decays with distance from the source. The theory can also be interpreted in the context of a time-dependent planar flow. When many parcels of lava participate, the overall shape of a one-dimensional lobe has the appearance of a continuum wave. The types of processes contained in the random walk model explain the multitude of concurrent or overriding features found in broad fields of toes. The basic formalism can thus be extended to simulate large fields of emplaced pahoehoe in either terrestrial or planetary settings.

1. Introduction

Broad pahoehoe flow fields, such as shown in Figure 1, are generally complex collections of much smaller, sometimes amorphous features. Such pahoehoe flow fields are often built up by the emplacement of these small features at many different locations sequentially or simultaneously. They may be interspersed with a'a lobes in a complex time-sequencing of emplacements [e.g., Nichols, 1936; Walker, 1972; Swanson, 1973; Holcomb, 1976]. The fact that flow fields are not comprised of a handful of simple discrete flow units, like well-defined and isolated a'a lobes, makes the emplacement process extremely difficult to model. Thus, to better understand the flow fields as a whole, we begin by investigating the emplacement of typical small features observed within flow fields. The ultimate objective of this work is to eventually simulate large flow fields for comparison with image and topography data for lava flows on Earth and other terrestrial planets.

When one observes the emplacement of pahoehoe toes, amorphous fields of toes, and certain kinds of lobes, it becomes immediately evident that a host of random processes influence emplacement. These random influences may include topographic variations at a variety of scales and small-scale random processes associated with the

cooling, cracking, and stretching of the outer skin. There are also local random effects associated with budding, channel, and lobe formation, interactions with active or emplaced parcels, and fluctuations in the supply and distribution of lava.

There are, of course, systematic and deterministic influences on pahoehoe emplacement as well. While fluid, a parcel of lava will tend to flow downslope. While in motion, a fluid element carries momentum and is subject to forces from neighboring elements or boundaries. One would hope to model pahoehoe emplacement with a generalized Navier-Stokes equation, supplemented by governing equations for other processes such as heat transfer, phase changes, etc. However, we cannot apply such deterministic equations without modeling all of the small scale transport processes, topographic influences, and local fluctuations in lava supply and boundary conditions separately. In principal this may be possible, but it would be impractical to attempt a completely deterministic description of the complexity observed in the field. A stochastic formalism may be employed to describe both the deterministic and random influences that act simultaneously on the lava parcels.

We present here such a stochastic formalism that treats the transport of a parcel of lava as a random walk. But, what exactly does the term "random walk" mean? The classical approach to the development of a random walk treats a particle beginning at some initial location, then moving to all subsequent locations based on some prescribed set of probability laws. At any step, the movement of the particle to the next position is a random variable. On any particular step, or for any sequence of steps, the outcome cannot be predicted with complete certainty. All the movements of the particle have an element of chance that is described by probability concepts, rather than exact, deterministic ones.

There are many different types of random walks (e.g., classical uncorrelated Brownian motion, correlated, biased, Levy-flights, and fractal generalizations [see, for example: Chandrasekhar, 1943; Wax, 1954; Zauderer, 1983; Klafter et al.,1996; and references cited therein]). Some types of random walks are trivial to prescribe and apply to real physical processes. There are also cases where even the mathematical formalism defied exposition for almost fifty years [Goldstein, 1951; Zauderer, 1983]. Even though random effects tend to confuse initial observations in the field, it is clear that there are different styles of pahoehoe emplacement. At one extreme, a simple linear filament composed of a few toes may grow at the front, extending the filament by one unit. Then the process may be repeated. Figure 2 shows such an example. At the other extreme are the highly complex fields that may contain toes, lobes of toes, small sheets and channels, and other forms that are even difficult to name. In complex fields, toes, lobes, sheets, and channels can form concurrently and may override earlier features [Nichols, 1936; Walker, 1972; Swanson, 1973; Holcomb, 1976; Jurado-Chichay and Rowland, 1995; Crown and Baloga, 1999].

These different regimes of pahoehoe emplacement suggest that pahoehoe emplacement could be associated with different types of random walks. We formulate a very general random walk model for the movement of parcels of lava on a fixed spatial grid. This model determines the probabilistic distribution on the grid for different types of random walks. However,

one cannot determine the type of random walk applicable to different emplacement regimes from *a priori* theoretical considerations. This must be done by field observations and data/theory comparisons. Our model does not address the small-scale physics of budding and toe formation, but rather, focuses on the large scale movements of an ensemble of parcels.

The main step in any random walk formulation is to determine the probability distribution for the locations of a parcel or particle in space or time. Once this is done for a given random walk, all that can be known about single or multiple particle movements (e.g., means, standard deviations, moments) can be determined by computation. When multiple particles are released from the origin, this probability distribution determines the concentration of particles at any location in space or time. In our application, this probability distribution represents the thickness of a pahoehoe flow lobe.

Before presenting the random walk model, we first describe some specific pahoehoe features found at typical locations in Hawaii. We have studied features where the influence of random effects was at least as important as the deterministic ones. Given the wide variety of emplacement behaviors, we carefully define what we expect the random walk model to accomplish in the subsequent section. Next we formulate the emplacement of pahoehoe as a random walk characterized by two parameters. One parameter determines the degree of bias in the random walk, the other is a measure of the correlation between steps. Readers may be familiar with the simplest form of a random walk, uncorrelated Brownian motion [e.g., Chandrasekhar, 1943]. Our derivation is designed to contain uncorrelated Brownian motion as one limiting form. Our mathematical formulation extends this random walk so that a bias could be included that might serve to represent the tendency for movement in the downslope direction More importantly, our extension also includes the difficult concept of correlation among the steps of a random walk. This reflects a chain of memory in the movements of a parcel due to momentum and the influences of neighboring parcels. A key aspect of our general formulation is that it is set up recursively so that it can be applied repetitively to any number of steps or fluid elements.

For comparison, we have made observations and collected dimensional data on small pahoehoe lobes from many sites in Hawaii. We compare the qualitative predictions of the model for different types of random walks to what is seen in the field. We also compare measured cross-sections with theoretical predictions. It is shown that the correlated random walk describes a host of important features found in the field that cannot be explained by an uncorrelated random walk. As noted in the discussion, the theory can also be interpreted in the context of a time-dependent two-dimensional planar flow. When many parcels of lava participate, the overall time-dependent shape of a two-dimensional lobes has the appearance of a continuum wave. In conclusion, we identify some possibilities for future detailed data/theory comparisons and extensions to simulations of large pahoehoe fields.

2. Field Observations

We begin by summarizing our observations of active and inactive pahoehoe lava flows in Hawaii. The intent of our initial observations was to identify the qualitative

character of random effects on pahoehoe emplacement. These observations were expected to guide the development of a model of emplacement that would highlight the role of random effects. We have observed active toe emplacement at the current eruption of Pu'u O'o at Kilauea and numerous small inactive features on older flow units, including the 1969-1974 eruption of Mauna Ulu at Kilauea [Swanson, 1973; Holcomb, 1976], and prehistoric flows from Mauna Loa and Hualalai. We have looked at a range of small mappable pahoehoe units, comprised of apparently gas-rich to fully-degassed lava in a variety of settings, including steep and shallow slopes and different substrates [Wilmoth and Walker, 1993; Crown and Baloga, 1999].

For the purpose of developing a stochastic model, we have focused on a few simple features that permit us to describe the nature of the random effect. These features include isolated filaments of toes, monolayers of toes and similar mappable units [Crown and Baloga, 1999], and small lobes that were isolated, in pre-existing channels, or in contact with other lobes. Simple sheets of pahoehoe that appeared to have flowed as a single continuum unit according to classical viscous dynamics were not of interest for this study. Neither do we specifically address other formations, such as squeeze-ups from rifted tumuli, or overflows from channels [e.g., Jurado-Chichay and Rowland, 1995].

To develop precise objectives for a stochastic model, we must be clear about the feature definitions under study and their characteristics relative to the model. Our descriptions of units and observations are as follows:

Isolated filaments and monolayers:

Isolated filaments of a small number of toes, typically a few to about a dozen, are common in Hawaii (Figure 2). Often such a filament advances by budding from the forward toe, but toes may also form toward the side. There is random meandering as the filament advances but there is usually an overall directionality to the orientations of the toes. When unconfined by pre-existing topography, the thickness of such deposits is generally equivalent to one or two toes. It is not always possible to tell where the next toe will form or its orientation, or what the final shape of the filament will be. Such filaments are often found on steep local slopes (>15 degrees) and pali. The directionality of the filament generally aligns with the downslope direction, as would be expected, and the toes tend to be distended. However, isolated filaments are also found on small virtually flat slopes, yet they often retain a directionality. This may be due to the initial direction of lava from the source or the topographic slope at the scale of the toes or filament. In the field, such small-scale topography is often difficult or impossible to discern. On flat areas, emplacement may also take the form a broad sheet-like analog of a linear filament. This has been called a monolayer [Crown and Baloga, 1999]. Instead of a single strand, there is a broad sheet of toes that is typically one or two toes thick with a surface of mappable units.

Isolated and Laterally Confined Lobes:

We consider a lobe to be isolated if the margins were emplaced without obvious interference from pre-existing topographic influences (Figure 3). Isolated lobes are often composed of a few dozen to a few hundred parcels of lava. These parcels form toes, buds, and a variety of small mappable units when they are located at the outer surface of the lobe [Crown and Baloga, 1999] Lobes can take the

form piles that have transverse profiles with a central ridge, a crude bilateral symmetry, and a decay in the thickness of the deposit toward the margin. The lobate features we discuss here typically have a width of several meters to as much as ten meters and a length of about five meters to as much as a hundred. The outer surface of the deposit is composed of toes and there are often interior parcels of lava that never had the opportunity to form toes. Transverse thickness profiles initially seemed to be reminiscent of bell-shaped Gaussian cross-sections, modified by the the discrete nature of the toes themselves and the natural variability of the toe formation process. At a small scale, the lobe emplacement process is dominated by the formation of individual toes. However, at the scale of the lobe itself, the advancing motion may often resemble a continuum flow.

Where lobes are laterally confined, the cross-section shape tends to have a relatively flat centroid and a relatively rapid decay toward the margins. As with isolated lobes, this is sometimes reminiscent of a bell-shaped curve, although the toe formation process is not allowed to continue past the margins. Figure 4 shows a confined lobe where the lateral extent of the lobe was influenced by pre-existing topography. Unfortunately, "lateral confinement" is not always easy to distinguish in the field, as we initially preconceived. Based on a general qualitative survey of dozens of such features, it appears that the flow itself often provides its own lateral confinement through the emplacement of toes. This suggests that lateral self-confinement is as important, or perhaps even more important than the ambient topography in determining the cross-sectional shape of the deposit. Although more data is needed, we do not believe there is a systematic difference between the cross-sectional shapes of lobes that are confined and those that are not.

Broad amorphous fields:

Broad, complex flow fields result when multiple modes of lava emplacement occur within the same area or are superimposed on each other. Such fields may be composed of hundreds or thousands of toes, isolated and confined lobes, sheets, channels, and other features. When a broad field is still active, one can observe a toe form in one location while other toes intermittently form tens of meters away. As one area becomes inactive, others may become active at seemingly random locations in the field. This suggests very complicated spatially random lava transport patterns within the flow field (Figure 1).

3. Objectives for the stochastic model

If we must abandon a detailed deterministic approach to the emplacement process, one might reasonably ask, "What can we expect to accomplish with a stochastic model?" Based on the observations above, we have selected a limited set of tractable, practical objectives. The random walk model is expected to:

* Provide at least a qualitative description of the emplacement of monofilaments of small numbers of toes,

* Describe the spatial spreading rate of the margins when there are enough parcels to form a thin layer or lobe,

* Approximate quantitatively the shape of transects across lobes,

* Retain contact, under some set of parameters, with conventional descriptions of pahoehoe emplacement as a fluid dynamic and heat transfer process,

* Qualitatively describe transitions from emplacement regimes that are dominated by random motions to those that are coherent, organized, and subject to classical fluid mechanics, and,

* Suggest what should be measured in the field at length-scales comparable to toes and at length-scales comparable to flow lobes.

From a more altruistic perspective, we would like the random walk model to be based on sound probability theory. It should produce dimensions or features that can be compared with field data and contain the possibility of relating the parameters of the model to conventional physics of mass, momentum, or heat transfer. We can of course simulate any sequence of random events on a computer provided enough decision criteria are built into the simulation. We would like the model to provide a general means for discriminating whether a particular simulation is representative or not.

4. The Correlated Random Walk Model

To formulate and interpret a random walk model of lava flow emplacement, we must be specific about the definition of a "parcel" of lava. A parcel is considered to be a fixed volume of lava that is sufficient to form a typical toe or some other form of discrete mappable unit. While in motion, possibly within a much larger ensemble of such parcels, it may be a fluid element that actually bears no resemblance to its final form. We do not suggest that all parcels become toes, but merely use such a concept as a convenience. In our work here, we treat parcels as having a single volume. Statistical variations in parcel dimensions in Hawaii and Idaho are given in Crown and Baloga [1999], but such differences are not treated here.

Based on field observations, it is clear that the random walk formalism must include the possibility of a bias. Such a bias represents a tendency for motion to occur in a preferred direction. For example, an isolated parcel may tend move in the direction of the downslope gradient. Also, parcels may carry momentum and be influenced by prior motions and source conditions. These processes are more closely associated with the concept of a correlation between movements rather than a bias. So, the model should also incorporate the possibilities of perfect correlation, its absence, and the full range of intermediate cases. To be useful for simulating large flow fields, or planetary scale settings, the theory must be applicable to a full range of scales from a few toes to thousands of parcels. We desire a general analytic formalism that would allow us to relate the model to conventional fluid dynamics. Finally, for practical reasons, the formulation must avoid having to manually derive the probability distribution for each step for different degrees of correlation or bias.

Our formulation of the correlated random walk uses two parameters to describe different types of random walks on the grid shown in Figure 5. See Table 1 for a definition of mathematical symbols. The first parameter α is the probability of taking an

upward (+y) step from any location when the choice is random. Thus, 1-α is the probability of taking a step in the downward (-y) direction. When $\alpha = 0.5$, the random walk is said to be unbiased.

We also use a parameter ρ that provides a measure of the correlation in the random walk and the amount of randomness. When $\rho = 0$, the random walk is said to be uncorrelated. This means that the tendency of move upward or downward at any step is governed solely by α and is completely independent of any choices made on prior steps. When $\rho = 1$, there is no randomness except for the first step. We refer to this case as perfect correlation. Once a parcel starts in a direction, it continues identically in that same direction. In general, for arbitrary combinations of the parameters, a random walker can be at any y-value from -N to +N after N steps. We seek a general formulation for any combination of α and ρ values.

The objective is now to determine the explicit form of P(y, N), the probability that a parcel is located at a position y on the grid after N steps have been taken. We use a recursive matrix formulation that determines the probability distribution after N steps based on the distribution after N-1 steps:

$$(y,\ N)] = [\Lambda(N)][P(y,\ N-1)],\quad N \geq \quad \textbf{(1)}$$

The key to such a formulation is finding the form of the [N-1 x N] matrix [Λ (N)]. Once [Λ (N)] is determined explicitly, eq 1 can be used to obtain the probabilities at any step for any mixture of bias and correlation. The recursive process is started by specifying [P(y, N=1)] with the two elements P(y=+1, N=1) =α and P(y=-1, N=1) = 1-α. All subsequent probabilities are then found by repeated applications of eq 1.

Determining the explicit form of [Λ (N)] was very challenging because the correlations originate directly from two prior steps, and indirectly from all prior steps, while the recursion relation is based only on the immediately prior probabilities. As part of this determination, we must also ensure that (1) the probabilities retain normalization: $\sum P(y;N)=1$ at each step, (2) for $\rho=0$, we recover the classical binomial distribution describing an uncorrelated random walk with an arbitrary bias, and (3) when $\rho=1$ the initial motions are retained identically.

For P(y, N) to be a rigorous probability, it must satisfy the normalization requirement (1). This imposes constraints on the elements of the matrix [Λ]. If we require

$$\sum_{j} \Lambda_{j,k}(N) = 1 \qquad \textbf{(2)}$$

i.e., the elements of each column sum to 1, then P(y, N) will be normalized if P(y, N-1) is normalized. This is proven by summing all the P(y, N) on the left side of eq 1, writing out the right hand side explicitly, and using eq 2. Thus,

$$\sum_{-N \leq y \leq N;\ (y,N)\ \text{same parity}} P(y,N) = \sum_{-N+1 \leq y \leq N-1;\ (y,N-1)\ \text{same parity}} P(y,N-1) \qquad \textbf{(3)}$$

So, once we assure that the probabilities of the first step are normalized, the probabilities of all subsequent steps will be guaranteed if the elements of [Λ] satisfy eq 2.

The requirement (2) to reproduce an uncorrelated random walk means the elements of [Λ] must make:

$$P(y;N) = W(k,N,\alpha) = W((N+y)/2;\ N;\alpha) = \frac{N!}{[(N+y)/2]![(N-y)/2]!}\ \alpha^{\cdot}\ (1-\alpha)^{\cdot} \quad \textbf{(4)}$$

when $\rho = 0$. Here W is the binomial distribution for k= (y+N)/2 successes out of N Bernoulli trials with success probability α. It is interesting to recall here that the limit of the binomial distribution as N becomes large is the classical Gaussian or normal distribution that describes bell-shaped curves. Our requirement (3) to retain initial motions identically when $\rho = 1$ means that [Λ] must make: P(y=+N, N)=α and P(y=-N, N)= 1-α for the case of perfect correlation.

We have derived the general form of [Λ (N)] by analyzing the grid in Figure 5 and the three requirements above. Now we indicate, by example, how the matrix elements were obtained. Correlation is, in effect, memory of the choice made by a parcel in the prior step to travel upward or downward. Thus, it first becomes evident on step N = 2. So, the first task is to obtain Λ (N=2) from the three requirements and the recursion relation:

$$[P(y,\ 2)] = [\Lambda(2)][P(y,\ 1)] \quad \textbf{(5)}$$

The derivation of the six elements of [Λ (2)] is easily illustrated by the tabular form:

P(+2, 2)		Λ_{11}	Λ_{12}	P(1,1) = α
P(0, 2)	=	Λ_{21}	Λ_{22}	P(-1,1) = 1-α
P(-2, 2)		Λ_{31}	Λ_{32}	

If we examine Figure 5, we see that the parcel cannot travel to y=+2 if the first step was downward or y = -2 if it originally went upward. Consequently $\Lambda_{12} = \Lambda_{31} = 0$. If a parcel travels to y=+2, it must have probability α^2 when $\rho = 0$ and probability α when $\rho = 1$. This can be obtained by setting $\Lambda_{11} = \rho+\alpha(1-\rho) \equiv p^{++}$. Here we introduce the superscripts because these elements will appear elsewhere in the general matrix for [Λ(N)]. To satisfy the normalization condition of requirement (1), this further implies $\Lambda_{21} = 1 - \rho - \alpha(1-\rho) \equiv p^{+-}$. By similar analysis of y = -2, we must set $\Lambda_{32} = 1- \alpha (1-\rho) \equiv p^{-}$ to obtain the probability $(1-\alpha)^2$ when $\rho = 0$ and probability 1-α when $\rho = 1$. Then normalization requires $\Lambda_{22} = \alpha(1-\rho) \equiv p^{-+}$.

All six of the elements of [Λ (N=2)] have thus been determined explicitly in terms of the two parameters α and ρ. It is easy to verify that the P(y, 2) sum to 1 for any combination of α and ρ, the binomial distribution is obtained for $\rho = 0$, and P(y=+2, 2)=α and P(y=-2, 2) = 1-α when ρ = 1.

The same seemingly simple process can be used to obtain [Λ (N=3)] and [Λ (N=4)]. However, as the reader may wish to verify, the derivation rapidly becomes much more complex. Unforeseen problems arise with the edge effects, counting the central paths correctly, and retaining normalization of P(y=3, 3) and P(y=4, 4). Only when N $\geq$ 4, do we appreciate the full difficulty of the problem. How this occurs can be seen from Figure 5. If we take an arbitrary location on the grid, we see that there are, in general, four possible locations that can result in the two subsequent steps. Consequently, if we use the mirror image of such a wedge, we impinge on the boundary in different ways coming backwards from step 4 to step 2.

We have found, nevertheless, our main theoretical result to be the general explicit form of [Λ (N)] as:

p^{++}	0	0	→		0
p^{+-}	p^{-+++}	0			
0	p^{--+-}	p^{-+++}			
0	0	p^{--+-}	↘		
↓			↘	↘	
				p^{--+-}	p^{-+}
0				0	p^{--}

where the probabilities p^{-+++} and p^{--+-} are defined in Table 1. We note that this matrix always has dimensions of [N-1 x N], and that only the diagonal elements shown contain non-zero values.

By using this result in eq 1, we can readily generate the probability that a parcel will be located at any admissible y-value after N steps. It is straightforward to show that all three requirements are met in the general case by using the explicit elements for the [Λ (N)] from Table 1. This general form for [Λ (N)] is the main result of the theoretical formulation. With it, we can obtain the distribution of an ensemble of parcels for any desired combination of bias and correlation. When many random walkers are considered, the thickness of a lobe is considered to be proportional to the probability that a single random walker is at location y at step N.

5. Applications

Monofilaments:

The simplest application of the random walk formalism is the advance of a monofilament. We show this trivial case to illustrate future possibilities for more detailed simulations. Here our goal is to model the meandering of the strand. We do not consider here the possibility of budding at locations other than the toe, although this clearly occurs in the field. As a toe forms at the front of its predecessor, it is considered to take a single step in the x-direction. Simultaneously the parcel is also considered to take a random step in either the plus or minus y- direction. A filament of N toes is thus formed by a sequence of N random steps. The process of simulating a monofilament corresponds to generating a single path in the network shown in Figure 5.

As an example, we suppose that an x, y coordinate system is laid out in an arbitrary direction and that 8 toes are to be emplaced along the path of the random walk. We consider the random walk to be uncorrelated but biased with $\alpha = 0.75$. This means the probability of taking a step in the +y direction is 0.75 and the probability of taking a step in the -y direction is 0.25 for each step of the sequence. On the average the monofilament has a constant drift along our coordinate system as long as α is constant. In our example, the average step is then $\langle y \rangle = 0.5N$, and thus, after 8 steps we expect the tip of the filament to be at y=+4.

We have simulated such paths with a random number generator by setting

$$\Delta y_i = \epsilon \quad \forall\, i \qquad (6)$$

where the ϵ are taken from a Bernoulli distribution with $\langle y \rangle = 0.5$. It should be note that many random number generators produce the Bernoulli distribution P(z) for $z \in [0, 1]$. To convert this to our y coordinates, we use the transformation

$$y=2z-1, \quad \bar{z}=\frac{\bar{y}+1}{2} \qquad (7)$$

Results of these simulations are shown in Figure 6. The straight line shows the average path. Other paths correspond to different simulations with the same parameters. It is very clear that any particular sequence may have a very different shape from the average. The randomness in the toe orientations is evident, as well as the influence of the bias in each step. Physically the randomness in the orientation could be related to the location of the budding site, while the bias could be due to the overall downslope direction with respect to our coordinate system.

This trivial example reflects qualitatively the monofilament meandering found in the field. Field studies of such orientations could be performed. However, we anticipate that little would be gained because this style of emplacement is dominated by the detailed microphysics of the budding process and the stochastic formulation is directed towards larger ensembles. We leave it to the interested reader to determine the variance or standard deviation of this application and its conversion into the distribution of orientation angles. The interested reader may also wish to tackle similar simulations with the correlated random walk

$$\Delta y_i = (1-\rho)\,\epsilon + \rho\,\Delta y_{i-1} \quad \forall\, i \qquad (8)$$

and investigate the influence of correlation on the angular distributions of orientations. Clearly, the discrete steps of our trivial example can be extended to continuous distributions as given in Crown and Baloga [1999].

Lobes:

An isolated lobe is produced by the model when there are enough parcels to form a distribution P(y, N) at all accessible y values after N steps. Thus the lobe will have relief and some shape in cross-section. When correlation is absent, the result is the cross-section given by eq 4. Figure 7 shows typical theoretical transects for the uncorrelated random walk at three different advancing steps of lobe emplacement.

We have visited numerous sites at Kilauea, Mauna Ulu, Haulalai and various other locations in Hawaii, where lobes are readily found on the flow fields. We found that isolated lobes sometimes have a mild medial peak with an approximately symmetric decay toward the boundaries. Sometimes transects are reminiscent of the bell-shaped curve. Our initial qualitative inspections of isolated lobes suggested that the emplacement process might simply be an uncorrelated random walk. These qualitative observations also suggested that a more quantitative data-theory comparison was desirable.

Figures 8a and b show transverse thickness profiles for two typical lobes at Hualalai. The measurements were obtained by stretching a leveled rope above the lobe, perpendicular to the general direction of flow, and measuring the relief to the nearest centimeter at evenly spaced intervals. Because the surfaces of the lobes are irregular, a replicate transect was measured at the same station in each case to indicate the natural variability.

We have collected about two dozen such transects to see if the hypothesis of an uncorrelated random walk was consistent with

the data (Figure 8). These figures do indeed show a crude connection with the measured transects and the theoretical cross-section associated with an uncorrelated random walk. However, the most striking difference one observes in the field is that the lobes are generally flatter on the top than one might attribute to a Gaussian. Although the random walk approach seemed promising, the most elementary uncorrelated form does not provide a good quantitative or qualitative comparison with field transects.

It is not completely surprising that the applicability of the uncorrelated random walk to pahoehoe transport is limited. First, this classical random walk minimizes the interaction between parcels during transport. Thus, the limited influence of neighboring parcels precludes the application of conventional fluid dynamics to the entire active lobe. If the uncorrelated walk was always valid, we would have to abandon all conventional viscous fluid dynamic models except for a parcel-by-parcel applications. A second problem with the uncorrelated random walk became evident from computer simulations of many uncorrelated random walks. These simulations superimposed many monofilaments. They reproduced broad, amorphous flow fields of many thousands of parcels, but were far too diffuse to represent solitary or multiple lobes.

We have addressed these issues by considering the correlated random walk. With a correlated random walk, some "memory" of what happened to a parcel at prior steps is retained. Correlation is a manifestation of the momentum of the flow, inertial effects, and fluid dynamic pressure when there are many contiguous parcels in a flow lobe.

Figures 8a and b also show the theoretical cross-sections when correlation is present. The flatness of the shape that corresponds to what is typically observed in the field is obtained when the correlation parameter ρ is in the vicinity of 0.25 to 0.30. For lesser values, the cross-sectional shape is more leptokurtic. Although the flatter cross-sections are typical, some lobes do show a modest medial peakedness.

Figure 9 shows the distribution of pahoehoe parcels for a higher level of the correlation parameter ρ. The profiles are shown at subsequent time steps from 5 to 20 with ρ =0.55. Two noteworthy features are evident. First, correlation at this level produces noticeable lateral margins in the upstream region. The shape of the margins clearly indicates a tendency of the flow to channelize as a direct result of the correlation. Such an effect has been documented [Crown and Baloga, 1999] in field studies of the transitional regime from discrete pahoehoe toes to larger units. Such flow margins cannot be produced by an uncorrelated random walk without lateral topographic confinement. Second, the influence of the correlation eventually decays for sufficiently long distances from the source. After 20 steps, all influence of correlation has been lost and the transect cannot be distinguished from a normal distribution. Qualitatively, this is what is often observed in the field. At the front of a small lobe, there can be budding and the random formation of new units while lava transport upstream is more coherent.

With an uncorrelated random walk, all the influences on the formation of a toe or the transport of a parcel are local. The uncorrelated random walk describes a number of qualitative features observed in the field, such as the meandering of isolated filaments and the budding of toes. This model seems to

be adequate for a small number of toes, say less than about a dozen, that occupy a single path on the grid. The uncorrelated random walk predicts a medial thickening of the lobe in cross-section with a gradual decay to the margins, which is not the typical case observed in the field.

The influence of correlation becomes a significant effect in the transport of pahoehoe as the number of parcels increases and large-scale fluid dynamic effects compete with the random processes. As with the classical correlated random walk [Zauderer, 1983], our formalism also shows that any correlations due to pressure, momentum, and inertia must eventually decay. In the continuum limit for very large numbers of parcels, correlated random walks engender wave equations [Zauderer, 1983; Goldstein, 1951]. These wave equations, in turn, can naturally describe surface wave structures and lobate features at the fronts and margins, as is often seen in terrestrial and planetary lava flows. From classical statistical physics [cf Zauderer, 1983 and refs therein], correlation can be associated directly with the terms used for viscous fluid flow. It also provides a "chain of memory" between downstream parcels and the source of lava supply. In effect, the correlated random walk provides a bridge between random effects at the toe or parcel-scale and large-scale continuum fluid dynamics.

6. Discussion

It must be admitted that a possibility for obtaining better agreement of the uncorrelated random walk with field observations is by lateral confinement at the margins. Whether by pre-existing topography, or perhaps by the cooling of the outermost lateral boundaries, the effect would be to thicken the margins, thus flattening the cross-section. For completeness, we now determine the transect shapes that are produced by a laterally confined uncorrelated random walk.

We suppose there is some confining boundary on one side at y_o . When uncorrelated random walkers encounter this boundary, they are reflected back into the admissible parts of the network and resume their random walk. Chandrasekar [1943], with reference to Smoluchowski [1915], uses a clever analysis of the image of paths beyond the reflecting boundary to show that, for a single reflecting plane at $+y_o$,

$$P(y;N) = W((N+y)/2;\ N;\alpha) + P(2y_o - y;\ N)\ W((N+y)/2;\ N;\alpha) + W((N+2y_o - y)/2;\ N \quad (9)$$

It is straightforward both conceptually and analytically to verify that the probabilities given by eq 9 retain normalization.

We have used this approach with two reflecting boundaries at $+y_o$ and $-y_o$ to represent the lateral confinement of lobes. To use this formula, one must be careful about a number of details. For example, on the array we have specified, the sites that are accessible depends on whether N is even or odd. For N=even, y must be even, and the reflecting boundary must be from the prior step. This means the boundaries for lateral confinement must be at odd locations. For N=odd, these considerations reverse. The lateral confinement of the random walk has the effect of trimming off the tails by shifting the parcels to admissible interior parts of the distribution. Due to normalization, the effect is to steepen the sides of the distribution, thus flattening the overall shape. Figures 9a and b show two

transects that more closely resemble what is observed in the field.

At present, we cannot preclude the laterally confined uncorrelated random walk as a viable model for explaining the cross-sectional shape of pahoehoe lobes. However, there are three points that argue against it. First, the transects we have shown in Figures 8a and b represent typical cases. For the confined uncorrelated random walk to reproduce such shapes, approximately the same amount must be trimmed from the tails in actual lobes. As yet, we know of no physical mechanism that can cause this to be the usual behavior observed. Second, we would expect to find in the field a full spectrum of confinements, ranging from the Gaussian shape to extreme lateral confinements. This is not consistent with out observations, even when a pahoehoe lobe is found within embanking channels and between pre-existing flows. Third, it is physically appealing that, when enough parcels are present, and the random influences are relatively small, the lobe should be governing by classical continuum viscous dynamics. Such a limit cannot be attained by the uncorrelated random walk.

We now turn our attention to a time-dependent formulation of the random walk model for a 2-dimensional flow. Our purpose here is to illustrate how the parcel-scale considerations can be used to develop macro-scale governing partial differential equations. For simplicity, we use only the uncorrelated random walk. We now employ a continuum limit to show what happens when the number of parcels becomes infinitely large. In such a limit, the small-scale motions of individual parcels are considered beneath the resolution of the model and are indistinguishable. Thus, we observe only the overall evolution of the lobe or the flow field.

Mathematically, such a limit is obtained in the following way. We suppose that in a small quantity of time Δ, a parcel takes a step of length δ along the x-axis according to the Bernoulli distribution. We consider three bins at x-δ, x, and x+δ, and ask how the probability P(x,t) (or equivalently the total number of parcels) at x changes in the time Δ. The change is given by

$$\begin{aligned} P(x,\ t+\Delta)\ -\ P(x,t)\ = \\ \alpha P(x-\delta,t)) + (1-\alpha)P(x+\delta,t)\ - \\ (1-\alpha)P(x,t)\ -\ \alpha P(x,t) \end{aligned} \qquad \textbf{(10)}$$

If we expand this equation in a Taylor series that is first-order in time and second-order in space, we obtain, after taking the limits of the small quantities,

$$\frac{\partial P}{\partial t} + V\frac{\partial P}{\partial x} = D\frac{\partial^2 P}{\partial t^2} \qquad \textbf{(11)}$$

where

$$V = (1-2\alpha)\frac{\delta}{\Delta},\ D = \frac{\delta^2}{2\Delta} \qquad \textbf{(12)}$$

This is the classical diffusion equation with a kinematic transport term, where the diffusion coefficient D and the "wave velocity", V, are given in terms of the random walk parameters Δ and
δ. We can readily solve this equation for a constant flux at x=0. The time-dependent solutions are shown in Figure 11. In the continuum limit, even for the case of an uncorrelated random walk, we reproduce the shape of an advancing wave that looks much like what we would expect from conventional fluid dynamics. It remains for future

investigations to develop the correlated random walk in such a continuum limit.

Conceptually, we can now begin to interpret or simulate much of what is seen on the surface of broad, seemingly amorphous pahoehoe flow fields. The model represents several regimes of emplacement, including small monofilaments and monolayers of toes, small lobes that may have channels, and larger lobes that advance as a continuum wave. Flow fields are often superpositions of these different modes of emplacement. We do not at present know what controls the formation of one style of emplacement versus another. The quanitity, location, and timing of the lava supply are clearly a major factors. However, flow rate, cooling rate, texture, setting and gas content may all be important [Rowland and Walker, 1987; Rowland and Walker, 1990; Keszthelyi and Denlinger; 1996;Wilmoth and Walker; 1993; Crown and Baloga, 1999]. These, in turn, have there own random variations, which remain to be studied subsequently.

7. Conclusions

The transport and emplacement of pahoehoe often features random effects that compete with, or dominate, systematic effects. When such random effects are important, the use of a stochastic approach is necessary. This means that we can only predict dimensions, shapes, and features in a probabilistic sense. Even under identical starting conditions, particular realizations may differ from case to case. It is impossible to predict the details on any particular realization. Length and width become random variables, as well as any simulation of locations, thicknesses, etc. When the emplacement can be modeled as a random walk, the model provides a means for evaluating whether a particular case is representative or not.

The random walk theory we have presented embraces different types of random walks, biased, uncorrelated, and correlated. These three effects can be adjusted in the general case by two parameters, α and ρ.

The first parameter describes the pre-existing slope or other factors that bias the orientation of motion. The second parameter describes correlation between steps that is conceptually associated with momentum, inertia, and pressure effects. Small-scale pahoehoe features, such as monofilaments of toes and small lobes are amenable to description as different types of random walks.

We have collected field data intended to distinguish the different types of random walks for the small pahoehoe features found in flow fields. We have shown that an uncorrelated classical random walk does not completely describe what is typically observed in the field, except for the meandering of small filaments. Correlation must be added to the random walk to describe larger lobe cross-sections qualitatively and quantitatively. A special case of the uncorrelated random walk with lateral confinement can also reproduce the rather flat lobe thickness transects observed in the field. Although this special case cannot be rigorously precluded, a host of factors argue against its validity.

The correlated random walk provides an adequate description of lobe thickness transects and provides a conceptual bridge between random processes and conventional viscous fluid dynamics. It can be related to momentum transport, hydrodynamical fluid

pressure, and inertial effects, all of which operate to some extent when many lava parcels are contained in the active lobe. The natural spreading of a correlated random walk clearly has a channel-forming regime that decays to uncorrelated behavior far from the source, as is often seen in the field.

We have shown for the uncorrelated random walk how to obtain macro-scale governing partial differential equations from the random model at the lava-parcel scale when hundreds or thousands of parcels are involved in the emplacement. The time-dependent longitudinal transects thus obtained resemble the advance of a continuum wave. However, the more exciting prospect resides with the richness of possibilities, e.g., channels and wave-like structures, contained in the macro-scale correlated random walk.

The underlying physical processes and factors that determine the type of random walk in particular field settings are not yet understood. Future studies will focus on this connection, with emphasis on the transitions for one type of random walk to another and the explicit relationships to conventional lava transport models. The investigations reported here suggest that the random effects associated with pahoehoe emplacement are indeed amendable to quantitative treatment and offer promise for modeling the emplacement of planetary flows.

7. Acknowledgements

This work was completed with funding from the NASA Planetary Geology and Geophysics program. The authors wish to thank Drs. Paul Spudis and Benjamin Bussey for assistance with field measurements and Drs. David Crown and Scott Rowland for helpful discussions.

Figure Captions

Figure 1: A typical broad amorphous field of toes in Hawaii. This figure indicates the predominance of random effects on the emplacement process and the need for a stochastic approach.

Figure 2: An isolated filament formed by budding of toes. For the most part, the filament advances by the budding from the forward toe, but toes also form toward the side. There is random meandering as the filament advances but often a general overall directionality with randomness in the orientations of the toes.

Figure 3: A typical isolated lobe of pahoehoe toes. Note the thickening medial tendency and the decay toward the laterally unconfined margins. The transect shape is reminiscent of a bell shaped curve.

Figure 4: A typical laterally confined lobe. Here the lateral extent of the lobe was influenced by pre-existing topography.

Figure 5: 2-dimensional grid for the random walk. N and y are discrete variables representing the downflow distance and lateral distance respectively.

Figure 6: Simulations of a random walk for a monofilament. The straight line shows the average path. Other paths correspond to different simulations with the same parameters.

Figure 7: Typical theoretical transects for the uncorrelated random walk at three different advancing steps of lobe emplacement.

Figure 8 a, b: Typical examples of thickness cross-sections of isolated lobes at Hualalai. Each panel shows two replicate sets of measurements at the same station. Also shown are theoretical cross-sections with ρ=0.28 as solid line.

Figure 9: Theoretical cross-sections of lobes produced by a correlated random walk with ρ=0.45 at time steps ranging from 5 (top curve) to 20.

Figure 10 : Cross-sections of a laterally confined lobe and comparison with laterally confined uncorrelated random walk.

Figure 11: The wave formed by the advance of uncorrelated random walkers in the continuum limit. The two waves farthest right at t=75 and t=100 have α=0.9. The two waves to the left at t=75 and t=100 have α=0.75.

Table 1. Definition of Mathematical Symbols

Symbol	Definition
y	Distance from origin/flow center
N	Step number/downflow distance
$0 \leq \alpha \leq 1$	Single step probability (+y direction)
$0 \leq \rho \leq 1$	Correlation parameter
$[\Lambda]$	Recursion matrix
p^{++}	$\rho+\alpha(1-\rho)$
p^{+-}	$1-\rho-\alpha(1-\rho)$
p^{-+}	$\alpha(1-\rho)$
p^{--}	$1-\alpha(1-\rho)$
p^{--+-}	$(p^{--}+p^{+-})/2$
p^{-+++}	$(p^{-+}+p^{++})/2$
$W(k;\alpha, N)$	Binomial distribution for y successes in N Bernoulli trials with success probability α

References

Chandrasekhar, S, 1943, Stochastic problems in physics and astronomy. *Rev Mod Phys* **15**: 1-87.

Crown, DA and SM Baloga, 1999, Pahoehoe toe dimensions, morphology, and branching relationships at Mauna Ulu, Kilauea volcano, Hawaii. *Bull Volc* **61**:288-305.

Goldstein, S, 1951, *Q J Mech Appl Math* **4**:129-156.

Holcomb RT, 1987, Eruptive history and long-term behavior of Kilauea Volcano. US Geol Surv Prof Pap 1350, 261-350

Jurado-Chichay, Z, and SK Rowland, 1995, Channel overflows of the Pōhue Bay flow, Mauna Loa, Hawaii: examples of the contrast between surface and interior lava, Bull Vol, 57, 117-126.

Keszthelyi, L and R Denlinger, 1996, The initial cooling of pahoehoe flow lobes. Bull Voc 58, 5-18

Klafter et al., 1996, Beyond Brownian motion. *Physics Today* February, pp 33-39.

Nichols RL, 1936, Flow-units in basalt. J Geol 44, 617-630

Rowland, SK and Walker, GPL, 1987, Toothpaste lava: characteristics and origin of a lava structural type transitional between pahoehoe and 'a'a. Bull Volc 49, 631-641

Rowland, SK and Walker, GPL, 1990, Pahoehoe and 'a'a in Hawaii:volumetric flow rate controls the lava structure. Bull Volc 52, 615-626

Smoluchowski, M.v.,1915, *Wien Ber* 124, 263.

Swanson DA, 1973, Pahoehoe flows from the 1969-1971 Mauna Ulu eruption of Kilauea volcano, Hawaii. Geol Soc Am Bull 84, 615-626

Walker, GPL, 1972, Compound and simple lava flows and flood basalts. Bull Volc 54, 10-24

Wax, N, 1954, *Selected papers on noise and stochastic processes*, Dover Pubs, NY, pp 337.

Wilmoth, RA, and Walker GPL, 1993, P-type and S-type pahoehoe: a study of vesicle distribution patterns in Hawaiian lava flows, J Volc Geotherm Res 55, 129-142

Zauderer, E, 1983, *Partial differential equations of applied mathematics*, Wiley, NY, pp 779.

Figure 1

Figure 2

Figure 3

Figure 4

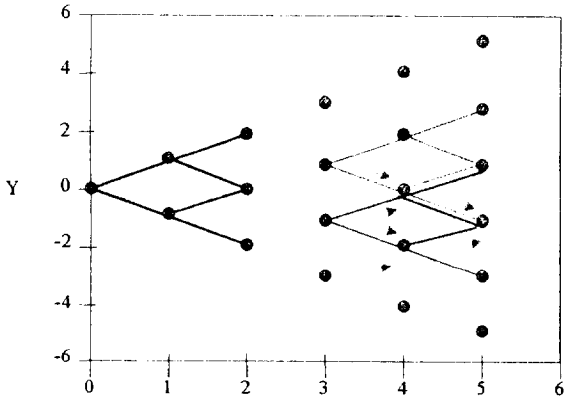

Figure 5

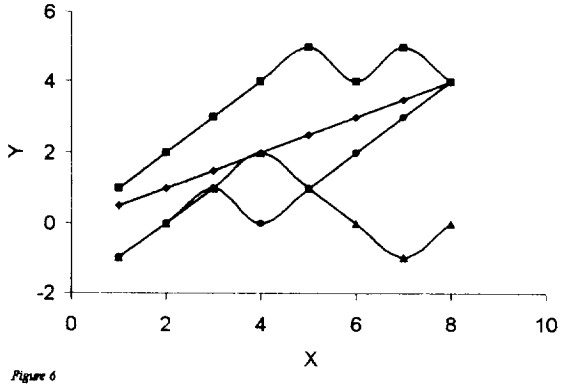

Figure 6

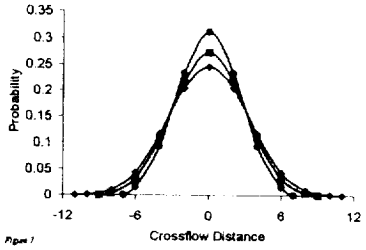

Figure 7

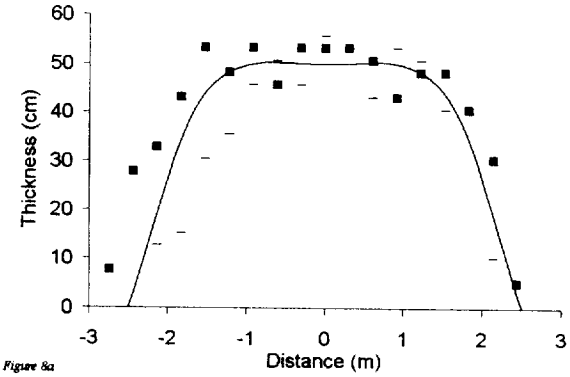

Figure 8a

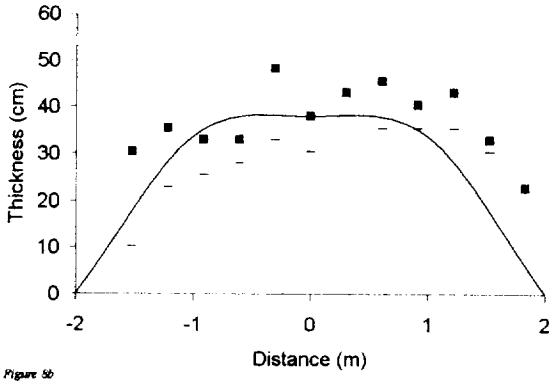

Figure 8b

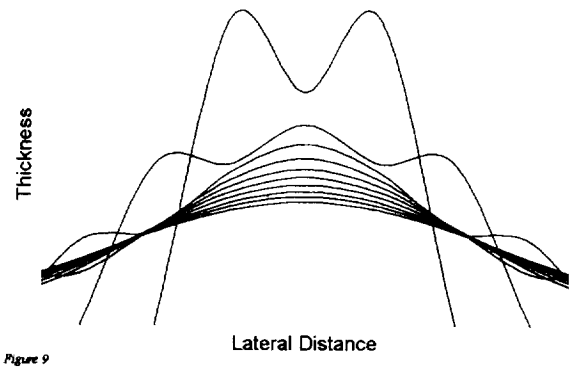

Figure 9

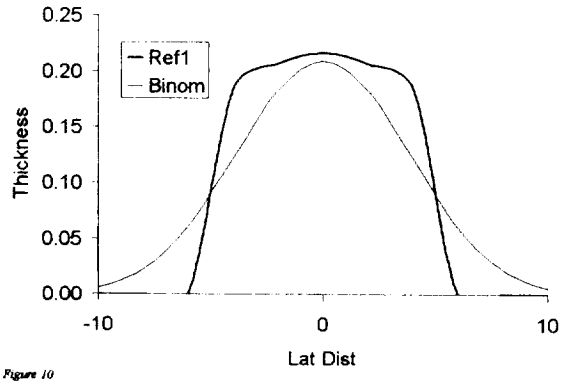

Figure 10

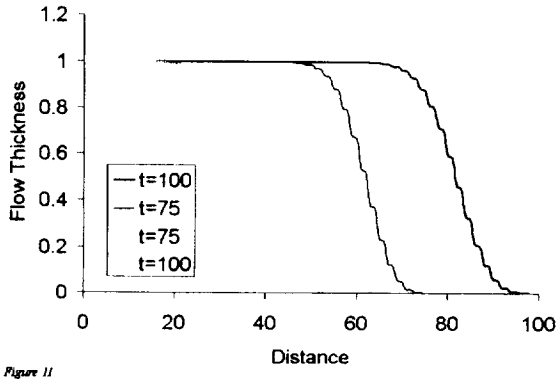

Figure 11

REPORT DOCUMENTATION PAGE

Form Approved
OMB No. 0704-0188

1. AGENCY USE ONLY *(Leave blank)*	2. REPORT DATE	3. REPORT TYPE AND DATES COVERED
	31 December 2001	Quarterly Report 10/1/01-12/31/01

4. TITLE AND SUBTITLE Quarterly Progress Report #101-004

5. FUNDING NUMBERS

C NASW-00013

6. AUTHORS Lori S. Glaze

7. PERFORMING ORGANIZATION NAME(S) AND ADDRESS(ES)

Proxemy Research
20528 Farcroft Lane
Laytonsville, MD 20882

8. PERFORMING ORGANIZATION REPORT NUMBER

IO 101-004

9. SPONSORING/MONITORING AGENCY NAME(S) AND ADDRESS(ES)

NASA
Code SR
Washington, D.C. 20546

10. SPONSORING/MONITORING AGENCY REPORT NUMBER

11. SUPPLEMENTARY NOTES

12a. DISTRIBUTION/AVAILABILITY STATEMENT

12b. DISTRIBUTION CODE

13. ABSTRACT *(Maximum 200 words)*

Proxemy Research is under contract to NASA to perform science research of volcanic plumes on Venus and Io. This report is submitted in accordance with contract NASW –00013 and contains a summary of activities conducted over the time period indicated in field 3, above. In addition to a synopsis of science research conducted, any manuscripts submitted for publication in this time period are also attached. Abstracts to scientific conferences may also be included if appropriate.

14. SUBJECT TERMS Venus/IO

15. NUMBER OF PAGES

16. PRICE CODE

17. SECURITY CLASSIFICATION OF REPORT	18. SECURITY CLASSIFICATION OF THIS PAGE	19. SECURITY CLASSIFICATION OF ABSTRACT	20. LIMITATION OF ABSTRACT
Unclassified	Unclassified	Unclassified	SAR